Check for updates

JGR Oceans

RESEARCH ARTICLE

10.1029/2024JC022068

New Insights on Dissolved Organic Matter Cycling in the Cape Verde Frontal Zone From Its Optically Active Fraction

R. Campanero Nieto[1,2], J. S. P. Ibanhez[1], B. Fernández-Castro[3], A. Martínez-Pérez[4], M. J. Pazó[1], V. Vieitez dos Santos[1], S. Valiente[5], M. Nieto-Cid[6], A. Delgado-Huertas[2], J. Arístegui[7], and X. A. Álvarez-Salgado[1]

[1]CSIC Instituto de Investigacións Mariñas (IIM–CSIC), Vigo, Spain, [2]CSIC-UGR Instituto Andaluz de Ciencias de la Tierra (IACT–CSIC-UGR), Granada, Spain, [3]Ocean and Earth Science, National Oceanography Center Southampton, University of Southampton, Southampton, UK, [4]Delegación del CSIC en Galicia, Santiago de Compostela, Spain, [5]Universidad de Granada, Granada, Spain, [6]Instituto Español de Oceanografía (IEO), Centro Oceanográfico de A Coruña, A Coruña, Spain, [7]Instituto de Oceanografía y Cambio Global, Universidad de Las Palmas de Gran Canaria, Telde, Spain

Key Points:

- Cape Verde Front and Cape Blanc Giant Filament dictate Dissolved Organic Matter optical properties distributions in epipelagic waters
- Local production of humic-like and consumption of protein-like substances occurs from sinking particle degradation
- Release from sinking particles leads to the accumulation of colored and fluorescent dissolved organic matter in the bottom nepheloid layer

Supporting Information:

Supporting Information may be found in the online version of this article.

Correspondence to:

R. Campanero Nieto and X. A. Álvarez-Salgado,
rcampanero@correo.ugr.es;
ruben.campanero@uam.es;
xsalgado@iim.csic.es

Citation:

Campanero Nieto, R., Ibanhez, J. S. P., Fernández-Castro, B., Martínez-Pérez, A., Pazó, M. J., Vieitez dos Santos, V., et al. (2025). New insights on dissolved organic matter cycling in the Cape Verde Frontal Zone from its optically active fraction. *Journal of Geophysical Research: Oceans*, *130*, e2024JC022068. https://doi.org/10.1029/2024JC022068

Received 6 NOV 2024
Accepted 30 JUN 2025

Author Contributions:

Conceptualization: A. Delgado-Huertas, J. Arístegui, X. A. Álvarez-Salgado
Formal analysis: R. Campanero Nieto, J. S. P. Ibanhez, B. Fernández-Castro, A. Martínez-Pérez, X. A. Álvarez-Salgado
Funding acquisition: A. Delgado-Huertas, J. Arístegui, X. A. Álvarez-Salgado
Investigation: R. Campanero Nieto, B. Fernández-Castro, S. Valiente,

© 2025. The Author(s).
This is an open access article under the terms of the Creative Commons Attribution-NonCommercial-NoDerivs License, which permits use and distribution in any medium, provided the original work is properly cited, the use is non-commercial and no modifications or adaptations are made.

Abstract Absorption and fluorescence spectroscopy have been used to gain new insights on the dynamics of Dissolved Organic Matter (DOM) in the Cape Verde Frontal Zone (CVFZ), a highly dynamic area comprising the thermohaline Cape Verde Front (CVF) and the Cape Blanc Giant Filament (CBGF), which exports organic matter produced over the shelf to the adjacent open ocean. A full-depth hydrographic box embracing the CVF and the CBGF was occupied in summer 2017 to examine the impact of these hydrographic structures and local-scale remineralization processes on DOM cycling using the distributions of the colored (CDOM) and fluorescent (FDOM) fractions of DOM as tracers. In the surface layer, we observed contrasting optical properties between the stratified, productive tropical waters south of the CVF with higher signals of optically active substances with higher molecular weight, and subtropical waters North of the CVF with lower signals and lower average molecular weight, pointing to lower microbial production and more intense or sustained photochemical degradation. In the ocean interior, although the mixing of intermediate and deep waters masses of contrasting origins and large-scale mineralization were the main factors controlling the distributions of the bulk and colored fractions of DOM, local-scale net accumulation of refractory humic-like and net consumption of labile protein-like components were observed in the mesopelagic layer. In bathypelagic waters, the optical properties of DOM allowed to characterize a bottom nepheloid layer (BNL) close to the Mauritanian coast, characterized by prominent CDOM and FDOM signals that were not noticeable in dissolved organic carbon (DOC) profiles.

Plain Language Summary The Cape Verde Frontal Zone is a highly dynamic region located between the Mauritanian coast and the Subtropical North Atlantic. It comprises the Cape Verde Front (CVF), where the North Atlantic and South Atlantic central waters meet, and the Cape Blanc Giant Filament (CBGF), which exports huge amounts of organic matter from the coast to the open ocean. At depths > 700 m, the area is a highway for intermediate and deep water masses coming from the Arctic to the Antarctic ocean. In this study we evaluate the role played by the dissolved organic matter (DOM) and its colored (CDOM) and fluorescent (FDOM) fractions in the biological carbon pump. The CVF and the CBGF determined the distribution and characteristics of the optically active DOM, discerning the productive coastal waters with higher rates of microbial production and higher molecular weight from the open ocean waters with higher rates of photochemical degradation and lower molecular weight. In the dark ocean, water mass mixing controlled primarily the distributions of CDOM and FDOM, but net production of recalcitrant DOM and net consumption of labile DOM was also observed. It is also noticeable the accumulation of CDOM and FDOM in the bottom nepheloid layer.

1. Introduction

Colored dissolved organic matter (CDOM) is the fraction of dissolved organic matter (DOM) capable of interact with light at visible and UV wavelengths and fluorescent DOM (FDOM) is the fraction of CDOM that emits part of the absorbed radiation in the form of blue fluorescence (Coble, 2007; Stedmon & Yamashita, 2024). These optically active fractions of DOM are useful tracers for ocean water mass mixing (Alvarez-Salgado et al., 2013; Kim et al., 2020) and biogeochemical processes, including phytoplankton exudation (Bachi et al., 2023; Romera-

M. Nieto-Cid, J. Arístegui, X. A. Álvarez-Salgado
Methodology: R. Campanero Nieto, B. Fernández-Castro, M. J. Pazó, V. Vieitez dos Santos, M. Nieto-Cid, J. Arístegui, X. A. Álvarez-Salgado
Project administration: J. Arístegui, X. A. Álvarez-Salgado
Supervision: A. Delgado-Huertas, X. A. Álvarez-Salgado
Visualization: R. Campanero Nieto, B. Fernández-Castro, S. Valiente
Writing – original draft: R. Campanero Nieto, X. A. Álvarez-Salgado
Writing – review & editing: J. S. P. Ibanhez, B. Fernández-Castro, A. Martínez-Pérez, M. J. Pazó, V. Vieitez dos Santos, S. Valiente, M. Nieto-Cid, A. Delgado-Huertas, J. Arístegui

Castillo et al., 2011), microbial processing of organic matter (Catalá et al., 2015; Kowalczuk et al., 2013; Xiao et al., 2023) and photochemical degradation (Helms et al., 2008; Timko et al., 2015; Yamashita, Boyer, & Jaffé, 2013). As a result of these processes, some recalcitrant colored and fluorescent fractions of DOM are consumed by microrganisms or photodegraded rapidly in the euphotic layer, producing smaller transparent organic carbon molecules, as well as carbon monoxide and dioxide (Del Vecchio & Blough, 2004; Swan et al., 2012; Twardowski & Donaghay, 2002). In this regard, two main groups of fluorophores are the most abundant in natural waters: protein-like, with emission wavelengths <400 nm (UV range) and associated to the labile free or combined aromatic amino acids tyrosine, tryptophane and phenylalanine, and humic-like, with emission wavelengths >400 nm (visible range), related to the recalcitrant humic and fulvic acids produced during organic matter degradation in soils or aquatic environments and that are highly sensitive to photodegradation (Coble, 2007; Stedmon & Nelson, 2015).

In this work we study the dynamics of the colored and fluorescent fractions on DOM in the complex and highly-dynamic Cape Verde Frontal Zone (CVFZ), located at the confluence of the North Atlantic Tropical and Subtropical zones, extending from Cape Verde archipelago (17ºN) to Cape Blanc (21ºN). This region is characterized by the presence of a persistent thermohaline front, created by the confluence of the saltier, nutrient-poorer and oxygen-richer East North Atlantic Central Water (ENACW) and the fresher, nutrient-richer and oxygen-poorer South Atlantic Central Water (SACW). This confluence feeds a rich meso- and submesoscale eddy field, which drives a vigorous exchange of salt, heat and nutrients (Campanero et al., 2022; Martínez-Marrero et al., 2008; Pelegrí & Peña-Izquierdo, 2015b; Pérez-Rodríguez et al., 2001; Zenk et al., 1991). The area is also affected by the Canary Upwelling system, where large amounts of organic matter, including its colored and fluorescent fractions, are generated and exported offshore to the open ocean through upwelling filaments, as the Cape Blanc Giant Filament (CBGF) (Burgoa et al., 2021; Gabric et al., 1993; Helmke et al., 2005; Lovecchio et al., 2018; Pelegrí et al., 2006; Santana-Falcón et al., 2020). This region is therefore acting like a gateway through which organic matter from the upwelling region accesses the open ocean, with important implications for the biogeochemical functioning of the adjacent gyre. Below this highly dynamic epipelagic layer, meso- and bathypelagic waters are characterized by their richness in water masses of contrasting origin and biogeochemical history. Apart from the ENACW and SACW that encounter at the thermohaline Cape Verde Front (CVF) and occupy the upper mesopelagic layer, three intermediate water masses are present in lower mesopelagic waters: Subpolar Mode Water (SPMW), with a Subpolar North Atlantic origin, Mediterranean Water (MW) and Antarctic Intermediate Water (AA) from the Subantarctic Front. In the bathypelagic layer, three water masses arrive to the area: Labrador Sea Water (LSW), and two branches (upper and lower) of North East Atlantic Deep Water (NEADW), originally formed in the Northern North Atlantic but mixed with different proportions of Antarctic Bottom Water (AABW) (Fernández-Castro et al., 2019; Pastor et al., 2015; Valiente et al., 2022).

The optical properties of DOM have been recently studied in this region by Campanero et al. (2022) and Devresse et al. (2023). The former reported the distributions of DOM and its optical properties at high resolution at the CVF, tracing meso- and submesoscale structures like eddies, fronts and meanders and showing the coupling between physical and biogeochemical parameters. In surface waters, the input of Sahara dust seemed to add highly re-worked fluorescent humic-like substances. In the dark ocean, mineralization processes lead to the production of refractory FDOM, primarily released from the fast-sinking POM. Devresse et al. (2023) studied the distribution of CDOM and FDOM in two eddies at high resolution off the coast of Mauritania, deciphering the DOM cycling in the area and how the eddies control biomass production and transport of nutrients and remineralized DOM. Contrary to these two studies, focused on the meso- to submesoscale, here we look at the regional scale variability covering the CVF and the CBGF, from coastal to open ocean and from surface to 4,000 m depth.

The hydrography and circulation (Burgoa et al., 2021) and the biogeochemistry of suspended and DOC and nitrogen (Valiente et al., 2022) have been recently studied in the CVFZ on the basis of the distributions obtained in a hydrographic box occupied during the FLUXES I cruise, in July-August 2017. This complementary study aims at achieving a deeper understanding of the origin, processing and fate of DOM in this buffering region, connecting the coastal productive waters with the adjacent oligotrophic ocean, using the absorption and fluorescence properties of DOM as tracers of these processes. These optical properties will also help us obtaining new insights about DOC export and DOM cycling in deep ocean waters of the study region.

21699291, 2025, 7, Downloaded from https://agupubs.onlinelibrary.wiley.com/doi/10.1029/2024JC022068 by Universidad De Las Palmas De Gran Canaria, Wiley Online Library on [01/08/2025]. See the Terms and Conditions (https://onlinelibrary.wiley.com/terms-and-conditions) on Wiley Online Library for rules of use; OA articles are governed by the applicable Creative Commons License

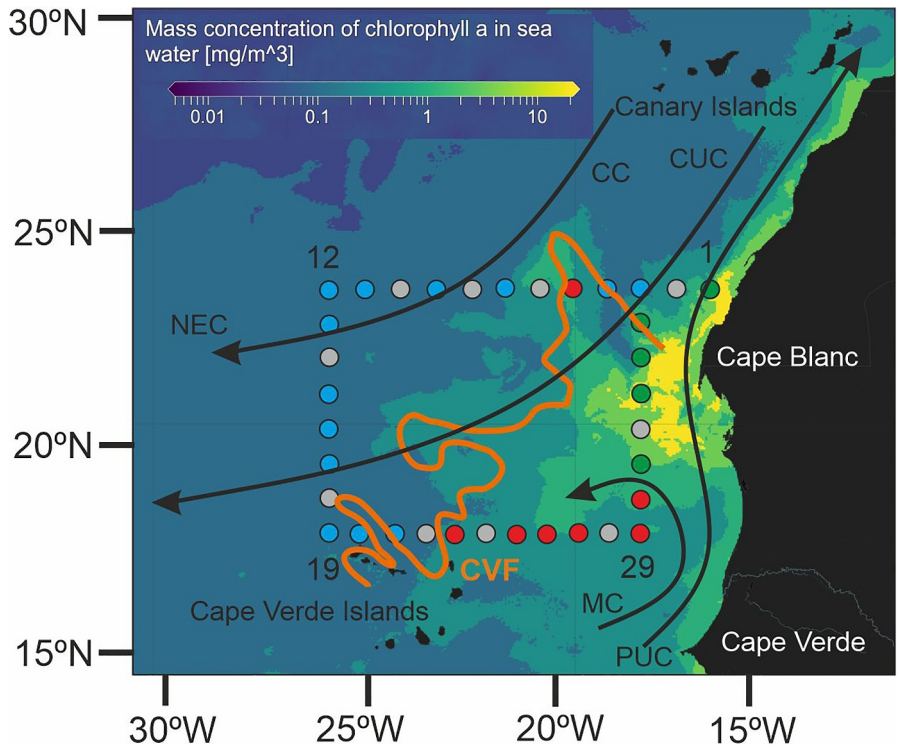

Figure 1. Map of the FLUXES I cruise over a remote sensing interpolated chlorophyll-a product from 25 July 2017, taken from Copernicus Marine Service, spatial resolution of 4 × 4 Km (https://doi.org/10.48670/moi-00281). The color dots represent the hydrographic stations where optical properties (CDOM and FDOM) were measured (blue: North of the CVF; red: South of the CVF; green: waters of the CBGF) and the gray dots are the stations without CDOM and FDOM measurements. Numbers indicate the station number from 1 to 35. Black arrows represent the Canary Current (CC), Canary Upwelling Current (CUC), North Equatorial Current (NEC), Mauritania Current (MC) and the Poleward Undercurrent (PUC) (taken from Pelegrí & Peña-Izquierdo, 2015a). The orange line represents the position of the CVF during the cruise (taken from Burgoa et al., 2021). For interpretation of the references to color in this figure, the reader is referred to the web version of this article. Adapted from Valiente et al. (2022).

2. Materials and Methods

2.1. Sampling Strategy and Analytical Procedures

The FLUXES I cruise took place from 12 July to 9 August 2017 on board R/V Sarmiento de Gamboa embarking and disembarking in Las Palmas (Canary Islands). Four transects defining a box were conducted off the coast of Mauritania in the CVFZ, with a total of 35 hydrographic stations 50 nautical miles apart (Figure 1). Transects were named as North, West, South and East, depending on their relative position in the box. Water samples were collected using a rosette sampler equipped with 24 Niskin bottles of 12 L. The rosette was also equipped with conductivity-temperature-depth (SBE911 plus), oxygen (SBE43), fluorescence of chlorophyll (SeaPoint SCF) and turbidity (SeaPoint STM) sensors. Sampling depth range covered down to 4,000 m in the medium and long stations (colored dots in Figure 1), and down to 2,000 m in the short stations (gray dots in Figure 1).

2.2. Core Variables

CTD conductivity, dissolved oxygen (DO) and chlorophyll (Chl-*a*) fluorescence sensors were calibrated using water samples taken from the rosette. Conductivity was calibrated with a Guildline 8410-A Portasal salinometer. Dissolved oxygen was determined using the Winkler potentiometric method with the procedure described in Langdon (2010). Apparent oxygen utilization (AOU) was calculated following Benson and Krause (UNESCO, 1986), where AOU = DOsat–DO (DOsat being the oxygen saturation concentration at local potential temperature and salinity, and DO being the measured value of oxygen). Chl-*a* was determined following the method of Holm-Hansen et al. (1965). For inorganic nutrients determination, 20 mL of water were collected in acid-cleaned polyethylene flasks and frozen at −20°C until colorimetric determination by segmented flow

21699291, 2025, 7, Downloaded from https://agupubs.onlinelibrary.wiley.com/doi/10.1029/2024JC022068 by Universidad De Las Palmas De Gran Canaria, Wiley Online Library on [01/08/2025]. See the Terms and Conditions (https://onlinelibrary.wiley.com/terms-and-conditions) on Wiley Online Library for rules of use; OA articles are governed by the applicable Creative Commons License

21699291, 2025, 7, Downloaded from https://agupubs.onlinelibrary.wiley.com/doi/10.1029/2024JC022068 by Universidad De Las Palmas De Gran Canaria, Wiley Online Library on [01/08/2025]. See the Terms and Conditions (https://onlinelibrary.wiley.com/terms-and-conditions) on Wiley Online Library for rules of use; OA articles are governed by the applicable Creative Commons License

analysis in the base laboratory following Hansen and Koroleff (1999). For DOC determination, pre-combusted borosilicate glass vials of 30 mL were used to collect and frozen the samples at −20°C, which were analyzed in the base laboratory, using a high temperature catalytic oxidation (680°C) total organic carbon analyzer model Shimadzu TOC-V. These samples were not filtered, but we named them as DOC because they mainly represent DOC due to the low concentrations of POC in oceanic waters. For more details on the analytical procedures, see Valiente et al. (2022). Statistical analysis of results was carried out using *t*-test to compare the means of different parameters.

The pycnocline was identified by the absolute maximum of the squared Brunt-Väisälä frequency, $N^2_{\max}$ (Doval et al., 2001). It was calculated as follows:

$$N^2_{\max} = g \cdot \frac{\ln\left(\rho_z/\rho_{z-1}\right)}{z-(z-1)} \quad (1)$$

where g is gravity acceleration (9.81 m s^{-2}), and ρ_z is water density at atmospheric pressure at depth z (in kg m^{-3}), calculated from salinity and temperature using the equation of (UNESCO, 1985).

2.3. CDOM and FDOM Determination

Water samples for the analyses of the colored and fluorescent fractions of DOM were taken from the Niskin bottles, collected in 250 mL acid-cleaned glass bottles and filtered through pre-combusted (450°C, 4h) 47 mm Whatman GF/F filters in an all-glass filtration system under a positive pressure of high purity N_2. Filtered seawater was stored in the dark allowing to warm up to room temperature until on board analyses in the respective measuring cuvettes of the spectrophotometer for CDOM and spectrofluorometer for FDOM.

Absorbance spectra of CDOM were recorded using a double-beam spectrophotometer Jasco V-750 from 700 to 250 nm at 0.5 nm intervals. The instrument was equipped with 100 mm path-length quartz cells and Milli-Q water was used as a reference blank. Absorption coefficient spectra $a_{\mathrm{CDOM}}(\lambda)$ (m^{-1}) were corrected by subtracting the Milli-Q spectrum and then applying the equation:

$$a_{\mathrm{CDOM}}(\lambda) = 23.03\ [\mathrm{Abs}(\lambda) - \mathrm{Abs}(600-700)] \quad (2)$$

where Abs(λ) is the absorbance at wavelength λ, Abs(600–700) is the average absorbance between 600 and 700 nm, which corrects for scattering primarily caused by fine particulate material and micro-air bubbles, and the factor 23.03 converts to natural logarithm and also considers the 0.1 m cell path length. The absorption coefficient indices used in this work were $a_{\mathrm{CDOM}}(254)$, $a_{\mathrm{CDOM}}(325)$, the ratio $a_{\mathrm{CDOM}}(254)/a_{\mathrm{CDOM}}(365)$, the spectral slope of the wavelengths bands 275–295 nm ($S_{275-295}$) and 350–400 nm ($S_{350-400}$), and the ratio of both spectral slopes S_R (Catalá et al., 2018; Coble, 2007; Engelhaupt et al., 2003; Helms et al., 2008).

Fluorescence excitation-emission matrices (EEMs) of the samples were recorded with a Perkin Elmer LS-55 spectrofluorometer using 10 nm excitation and emission slit widths, an integration time of 0.24 s, an excitation range of 240–450 nm at 10 nm increments and an emission range of 300–560 nm at 0.5 nm increments. Blanks were measured using freshly produced Milli-Q water following the same procedure. Processing of the EEMs started by subtracting the blank measurements from seawater EEMs. Afterward, the DOMFluor toolbox for Matlab (Stedmon & Bro, 2008) was used to cut Raman and Rayleigh dispersion bands. Then, EEMs were normalized to the Raman area, which was estimated applying the trapezoidal rule of integration (Murphy et al., 2010) on the emission scan at excitation 350 nm of the Milli-Q water blanks. Afterward, the absorbance spectra of each sample was used to correct the EEMs for inner filter effects (Kothawala et al., 2013). To test for instrument variability during the cruise, daily measurements were performed on a sealed Milli-Q cuvette (Perkin Elmer) to check for the Raman region, and p-terphenyl and tetraphenyl butadiene blocks (Starna) to check for protein- and humic-like substances regions, respectively (Catalá et al., 2015).

A parallel factor analysis (PARAFAC) was applied to decompose the fluorescence signal of the EEMs into the underlying individual fluorescent components (Bro, 1997). The PARAFAC was based on 294 corrected EEMs and performed using the DOM Fluor 1.7 and drEEM Toolboxes for Matlab. Five components were obtained (Figure S1 in Supporting Information S1) after validation through split-half analysis and random initialization

steps (Figures S2 and S3 in Supporting Information S1; Murphy et al., 2013; Stedmon & Bro, 2008). Components 1–3 (C1, C2, C3) correspond to humic-like substances, whereas components 4–5 (C4, C5) correspond to protein-like substances. The Excitation (Ex)/Emission (Em) maxima (in nm) of each component obtained by the PARAFAC is: C1 (240 (360)/450); C2 (310/405); C3 (280 (390)/485); C4 (270/355); and C5 (240/340), where the value in brackets for C1 and C3 indicates excitation maxima.

For each component, we report the maximum fluorescence (F_{max}) in Raman units (RU). The obtained C1 to C5 were compared to previous studies using the Openfluor database (openfluor.lablicate.com; Murphy, Stedmon, et al. (2014)). Components C1 to C4 were highly similar to several models included in the OpenFluor database (Tucker Congruence Coefficient of excitation and emission spectra >0.95; Table S1 in Supporting Information S1). No matches were found for component C5. C1 is a mixture of peaks A and C as defined by Coble (1996) and related to terrestrial humic-like substances. C2 is Coble's (1996) peak M, related to marine humic-like substances. C3 resembles peak D related to soil fulvic acids, that is of terrestrial origin (Stedmon et al., 2003). C4 is Coble's (1996) peak T identified as tryptophan protein-like substances and C5 could be a mixture of Coble's (1996) peak B identified as tyrosine protein-like substance and polycyclic aromatic hydrocarbons (PAHs) (Ferretto et al., 2014).

2.4. Water Mass Analysis

Any water sample is a combination of distinct proportions of different water types (WTs) which can be quantified with an optimum multiparameter (OMP) inverse method (Karstensen & Tomczak, 1998). A WT is characterized by a unique combination of thermohaline and chemical properties, which in this work are potential temperature (θ), salinity (S), silicate (SiO_4) and NO. The chemical parameter NO is defined as: $NO = O_2 + R_N \cdot NO_3^-$, with R_N = 9.3 mol O_2/mol NO_3^- (Anderson, 1995) being the stoichiometric coefficient of oxygen consumption to nitrate production. These WTs are end-members that demarcate water masses, which can be defined by one or more WTs. A total of 8 water masses defined with 11 WTs have been identified in the CVFZ: Madeira Mode Water (MMW); Eastern North Atlantic Central Water (ENACW) of 15°C and 12°C; South Atlantic Central Water (SACW) of 18°C and 12°C; Subpolar Mode Water (SPMW); Antarctic Intermediate Water (AA); Mediterranean Water (MW); Labrador Sea Water (LSW); and upper and lower North East Atlantic Deep Water (NEADW). While, MMW, SPMW, AA, MW and LSW are water masses defined by a unique WT, ENACW, SACW and NEADW are defined by two WTs. Thermohaline and chemical properties of these WTs are summarized in Table S2 of Supporting Information S1. The proportion of each WT (X_{ij}) in a given water sample can be obtained by solving a set of linear mixing equations for volume, θ, S, SiO_4 and NO in a non-negative less-squares sense. For further details, the reader is referred to Valiente et al. (2022). The water mass analysis includes samples below 200 m, where the variables used show a conservative or quasi-conservative behavior, contrasting with the epipelagic layer in which heat, mass and gases exchange with the atmosphere and biological activities preclude such a conservative behavior. A total of 236 out of 320 samples were selected for the determination of the relative contribution of each WT to each water sample in the mesopelagic and bathypelagic layers. The remaining 84 samples correspond to the upper 200 m.

Once the water type proportions (X_{ij}) are calculated, the archetype value (N_i) of any variable (N) in each water type is calculated as follows:

$$N_i = \frac{\sum_j X_{ij} \cdot N_j}{\sum_j X_{ij}} \quad (3)$$

where N_i represents the water mass proportion-weighted average concentration of N in every water type, X_{ij} is the proportion of WT i in sample j and N_j is the concentration of N in sample j. The standard error of the archetype value was obtained as:

$$SE_{N_i} = \frac{\sqrt{\sum_j X_{ij}(N_j - N_i)^2}}{\sum_j X_{ij}} \quad (4)$$

21699291, 2025, 7, Downloaded from https://agupubs.onlinelibrary.wiley.com/doi/10.1029/2024JC022068 by Universidad De Las Palmas De Gran Canaria, Wiley Online Library on [01/08/2025]. See the Terms and Conditions (https://onlinelibrary.wiley.com/terms-and-conditions) on Wiley Online Library for rules of use; OA articles are governed by the applicable Creative Commons License

21699291, 2025, 7, Downloaded from https://agupubs.onlinelibrary.wiley.com/doi/10.1029/2024JC022068 by Universidad De Las Palmas De Gran Canaria, Wiley Online Library on [01/08/2025]. See the Terms and Conditions (https://onlinelibrary.wiley.com/terms-and-conditions) on Wiley Online Library for rules of use; OA articles are governed by the applicable Creative Commons License

Archetype values were determined for Z, S, θ, O_2, AOU, DOC, CDOM ($a_{CDOM}(254)$, $a_{CDOM}(325)$, $a_{CDOM}(254)/a_{CDOM}(365)$, $S_{275-295}$ and S_R) and FDOM (C1-C5). Finally, the proportion of the total volume of the samples occupied during the FLUXES I cruise (%VOL_i) by a given water type i was calculated as:

$$\%\mathrm{VOL}_i = 100 \cdot \frac{\sum_j X_{ij}}{n} \tag{5}$$

where $n = 236$, is the number of samples collected below 200 m and included in the analysis. Note that %VOLi does not represent the effective volume of each water type in the study area, but of the water sampled during the curise, although Niskin bottle depths were decided to have representative volumes of the water types present in each cast.

To determine the fraction of the total variability of N due to water mass mixing, a multiple linear regression of N_j with the water types proportions (X_{ij}) is calculated:

$$N_j = \sum_j X_{ij} \cdot n_i + R(N_j) \tag{6}$$

where n_i is the slope coefficient for WT i and $R(N_j)$ is the residual of the equation for sample j. The determination coefficient (R^2) indicates the percent of the total variability explained by mixing and the standard error (SE) of the estimate defines the accuracy of the fit. This equation allows quantifying the impact of water mass mixing along with basin-scale mineralization on the distribution of the variable N (Alvarez-Salgado et al., 2013). Note that the multiple linear regression cannot be applied to $a_{CDOM}(254)/a_{CDOM}(365)$, $S_{275-295}$ and S_R because they are not concentrations but slopes or ratios.

To consider the combined effect of mixing and biogeochemical processes on the distribution of CDOM and FDOM signals, the explanatory variable AOU is added to the linear regression model (Equation 7), incorporating a coefficient (β) that relates the chemical variables (N) with AOU (Álvarez-Salgado et al., 2013, 2014; Valiente et al., 2022):

$$N_j = \sum_j X_{ij} \cdot n_i + \beta \cdot \mathrm{AOU}_j + R(N_j) \tag{7}$$

The coefficient β represents the ratio of the relationship between variable N and AOU, and more interestingly, is fully independent of water type mixing, something important in the Cape Verde Frontal Zone with so many water masses. Therefore, with Equation 7 it can be resolved the impact of large-scale (water type mixing, basin-scale mineralization) and local-scale mineralization processes on the distribution of any non-conservative variable as well as the corresponding stoichiometric ratios. Again, this multiple linear regression cannot be applied to $a_{CDOM}(254)/a_{CDOM}(365)$, $S_{275-295}$ and S_R.

3. Results

3.1. Hydrographic and Biogeochemical Variability in the CVFZ

3.1.1. Epipelagic Waters

The CVF is a thermohaline front that separates the warm and salty ENACW from the cooler and fresher SACW. It was first defined by Zenk et al. (1991) at the intersection of the 150 m isobath with the 36 isohaline. More recently, analyzing the FLUXES-I cruise data, Burgoa et al. (2021) extended this definition vertically and established an equation that defines the location of the front at any depth from 100 to 650 m, based on equal contributions (50%) of ENACW and SACW. We have used the latter definition of the CVF to classify the samples of the epipelagic layer (upper 200 m) into two hydrographic domains: (a) Subtropical, for the samples located to the North of the CVF, comprising most of the Northern and Western transects; and (b) Tropical, for samples located to the South of the CVF, that comprises mainly the Southern and part of the Eastern transect. Furthermore, a third domain consisting of upwelling filament waters, was identified. It was mainly located in the Eastern

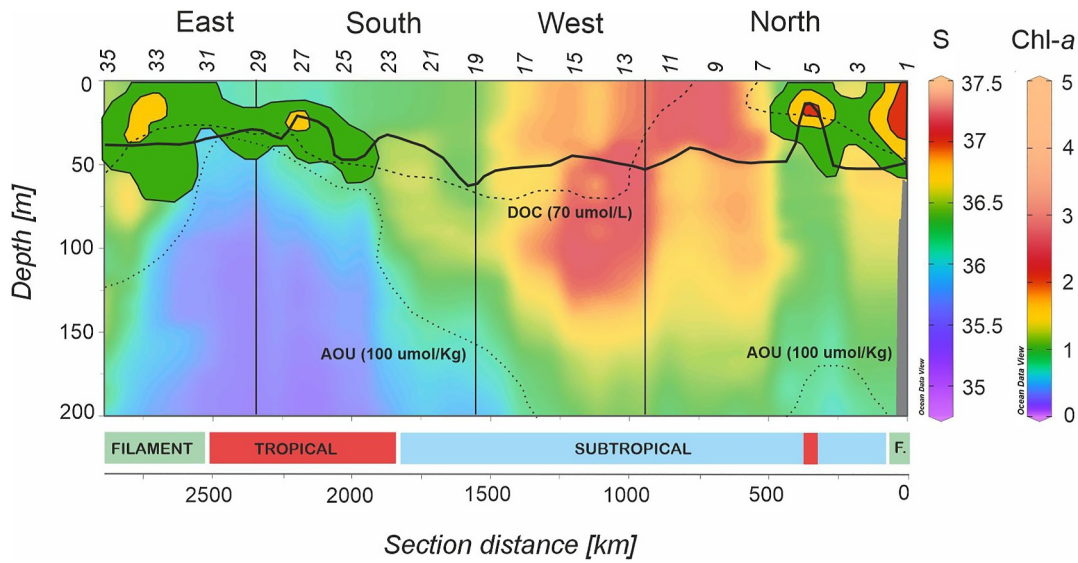

Figure 2. Distributions of salinity (S) (color shaded background) and chlorophyll-a (Chl-a) (solid color areas between stn 1–7 and 23–35) in μg L^{-1} in the epipelagic layer in July–August 2017. Dotted lines denotes the 70 μmol L^{-1} of dissolved organic carbon and 100 μmol kg^{-1} of Apparent oxygen utilization. The vertical resolution is 1 m. Horizontal black line shows the position of the pycnocline and the vertical black lines represent the corners of the FLUXES hydrographic box. F., filament. Odd station numbers are presented at the top of the panel. Produced with Ocean Data View (Schlitzer, 2017).

transect, comprising the stations affected by the CBGF, easily traceable by the satellite-derived surface chlorophyll distribution (Figure 1; see Valiente et al. (2022) for further details).

A well-defined pycnocline was identified along the four transects of the hydrographic box (see solid line in Figure 2). Deeper pycnocline depths were observed in the Subtropical domain with an average (SD) value of 51.2 (1.8) m. Shallowest depths were located in the Tropical domain with 33.6 (3.5) m. Finally, the pycnocline depth was 40.8 (1.9) m in the filament waters. Noticeably, the pycnocline at stn 5, in the Northern transect, was as shallow as 15 m because there was an intrusion of water from the Tropical domain at that position (Valiente et al., 2022).

The upper mixed layer of the subtropical domain was occupied by North Atlantic surface waters of higher salinity (average, 36.6; $p < 0.0005$) compared to the South Atlantic surface waters (average, 36.1), which prevailed in the Tropical domain (Figure 2, Table 1). Temperature differences across the pycnoline were higher (7.3°C) in the Tropical than in the Subtropical (4.0°C) domain. Consequently, the stability (N^2_{max}) (1.6 (0.1) 10^{-3} s^{-2}) was more than 3-fold higher than in the Subtropical domain (4.8 (0.1) 10^{-4} s^{-2}). Upper mixed layer temperature in the filament waters was lower ($p < 0.0005$) than in the Subtropical and Tropical domains, as expected for recently upwelled waters, and the temperature difference across the pycnocline was 5.0°C (Table 1).

The deep chlorophyll maximum (DCM) was located well below the pycnocline in the Subtropical domain, at an average depth of 75.8 (0.9) m, while in the Tropical domain the DCM was significantly ($p < 0.0005$) shallower, 37.9 (1.6) m, and much closer to the pycnocline. Conversely, in the filament domain, the DCM was shallower, 29.6 (2.0) m, and located above the pycnocline. Maximum Chl-*a* levels were observed in the Tropical and filament domains, corresponding with the shallowest DCM depths (Figure 2, Table 1). The Chl-*a* maximum at stn 5 corresponds to the already mentioned intrusion of waters with South Atlantic origin in the Northern transect (Valiente et al., 2022).

AOU above the pycnocline was positive (i.e., net community production is dominated by respiration processes resulting on net oxygen consumption) in the three domains, being significantly higher ($p < 0.0005$) in the Tropical and filament domains than in the Subtropical domain (Table 1). Differences were more pronounced below the pycnocline, where the AOU was higher in the less ventilated SACW of the Tropical and filament domains than the ENACW in the Subtropical domain. Finally, DOC presented higher concentrations in the surface mixed layer of the tropical domain with 87.0 (0.5) μmol L^{-1} ($p < 0.0005$). On the contrary, the highest

21699291, 2025, 7, Downloaded from https://agupubs.onlinelibrary.wiley.com/doi/10.1029/2024JC022068 by Universidad De Las Palmas De Gran Canaria, Wiley Online Library on [01/08/2025]. See the Terms and Conditions (https://onlinelibrary.wiley.com/terms-and-conditions) on Wiley Online Library for rules of use; OA articles are governed by the applicable Creative Commons License

21699291, 2025, 7, Downloaded from https://agupubs.onlinelibrary.wiley.com/doi/10.1029/2024JC022068 by Universidad De Las Palmas De Gran Canaria, Wiley Online Library on [01/08/2025]. See the Terms and Conditions (https://onlinelibrary.wiley.com/terms-and-conditions) on Wiley Online Library for rules of use; OA articles are governed by the applicable Creative Commons License

Table 1
Thermohaline and Chemical Characteristics (Average Value ± SE) of the Epipelagic Waters Above and Below the Pycnocline in July–August 2017 Along the Hydrographic Box

		Above pycnocline			DCM			Below pycnocline		
		Subtropical	Tropical	Filament	Subtropical	Tropical	Filament	Subtropical	Tropical	Filament
Z	(m)				75.8 ± 0.9	37.9 ± 1.6	29.6 ± 2.0			
θ	(°C)	23.3 ± 0.1	24.5 ± 0.1	21.9 ± 0.1	20.6 ± 0.0	20.3 ± 0.2	21.2 ± 0.3	19.3 ± 0.0	17.2 ± 0.1	16.9 ± 0.4
S		36.6 ± 0.0	36.1 ± 0.0	36.2 ± 0.0	36.7 ± 0.0	36.1 ± 0.0	36.2 ± 0.1	36.6 ± 0.0	36.0 ± 0.0	36.1 ± 0.1
Chl-*a*	(μg L^{-1})	0.24 ± 0.01	0.62 ± 0.03	1.28 ± 0.05	0.55 ± 0.01	2.07 ± 0.17	1.62 ± 0.20	0.32 ± 0.00	0.74 ± 0.04	0.29 ± 0.05
AOU	(μmol kg^{-1})	3.2 ± 1.1	8.7 ± 2.4	8.7 ± 2.0	15.1 ± 1.4	77.7 ± 5.7	11.8 ± 5.5	41.6 ± 0.8	128.8 ± 2.5	108.0 ± 11.3
DOC	(μmol L^{-1})	72.0 ± 0.2	87.0 ± 0.5	81.1 ± 0.5	63.9 ± 0.2	71.9 ± 0.6	77.9 ± 1.6	59.9 ± 0.1	60.8 ± 0.3	59.0 ± 1.2
$a_{CDOM}254$	(m^{-1})	1.31 ± 0.54	1.77 ± 0.01	1.61 ± 0.01	1.25 ± 0.01	1.59 ± 0.02	1.54 ± 0.04	1.15 ± 0.00	1.23 ± 0.01	1.15 ± 0.03
$a_{CDOM}325$	(m^{-1})	0.14 ± 0.002	0.31 ± 0.01	0.33 ± 0.01	0.19 ± 0.00	0.36 ± 0.01	0.33 ± 0.02	0.17 ± 0.00	0.25 ± 0.004	0.21 ± 0.005
*a*254/*a*365		26.56 ± 0.58	13.65 ± 0.40	9.64 ± 0.13	14.8 ± 0.2	9.1 ± 0.3	9.7 ± 0.5	14.61 ± 0.07	10.07 ± 0.11	10.70 ± 0.35
$S_{(275-295)}$	(10^{-2})	4.15 ± 0.03	3.33 ± 0.04	3.00 ± 0.12	3.58 ± 0.26	2.79 ± 0.46	2.96 ± 0.76	3.48 ± 0.01	2.79 ± 0.02	3.00 ± 0.06
$S_{(350-400)}$	(10^{-2})	1.86 ± 0.02	1.52 ± 0.01	1.30 ± 0.02	1.44 ± 0.15	1.30 ± 0.18	1.23 ± 0.35	1.37 ± 0.01	1.23 ± 0.01	1.26 ± 0.03
S_R		2.32 ± 0.02	2.20 ± 0.02	2.33 ± 0.02	2.55 ± 0.04	2.16 ± 0.03	2.44 ± 0.10	2.58 ± 0.01	2.27 ± 0.01	2.37 ± 0.01
C1	(10^{-3} RU)	11.2 ± 0.2	23.1 ± 0.6	27.6 ± 0.5	17.6 ± 0.3	31.8 ± 0.9	28.0 ± 2.1	17.4 ± 0.1	25.5 ± 0.3	21.0 ± 0.7
C2	(10^{-3} RU)	6.2 ± 0.2	12.8 ± 0.4	13.2 ± 0.3	10.1 ± 0.3	18.8 ± 0.6	14.7 ± 1.2	10.7 ± 0.1	15.9 ± 0.2	13.1 ± 0.4
C3	(10^{-3} RU)	2.9 ± 0.6	5.57 ± 0.1	7.27 ± 0.1	3.9 ± 0.1	7.2 ± 0.3	7.2 ± 0.5	4.2 ± 0.4	6.2 ± 0.1	5.4 ± 0.2
C4	(10^{-3} RU)	7.6 ± 0.1	14.3 ± 0.3	14.2 ± 0.3	6.7 ± 0.2	12.2 ± 0.6	11.7 ± 0.7	5.7 ± 0.1	6.8 ± 0.2	6.0 ± 0.5
C5	(10^{-3} RU)	15.0 ± 0.4	22.0 ± 1.5	10.1 ± 0.3	10.9 ± 0.5	7.2 ± 0.5	9.8 ± 1.1	8.6 ± 0.2	5.5 ± 0.2	3.6 ± 0.5

Note. Epipelagic waters are separated into three domains: Subtropical, Tropical and filament (see main text). Components C1, C2, C4 and C5 correspond with Coble's (1996) peaks A and C, peak M, peak T and peak B, respectively. Component C3 is similar to Stedmon's et al. (2003) peak D.

DOC value at the DCM was found in the filament domain with an average of 77.9 (1.6) μmol L^{-1}. Below the pycnocline, values decreased and were constant at about 60 μmol L^{-1} in the three domains (Table 1).

3.1.2. Ocean Interior

The hydrography of the meso- and bathypelagic layers of the CVFZ is controlled by the mixing of different water masses (Pastor et al., 2015) as shown in Figure 3. The average proportions of all water masses in each transect are summarized in Table S3 of Supporting Information S1. ENACW was present in similar proportions in the four transects whereas MMW concentrated in the Northern and Western transects, that is to the North of the CVF, and the SACW was ubiquitous in the Southern and Eastern transects, that is to the South of the CVF. At intermediate levels, while SPMW was present in the four transects, AA concentrated mainly in the Southern and Eastern transects and MW was dominant in the Northern transect.

Finally, both LSW and NEADW were present in the four transects, although shallower bottom depths in the Eastern transect led to a relatively smaller contribution of LNEADW. Weighted-average depths and percentages of sampled volume by every water type considering all transects together are summarized in Table 2. The most abundant water type in the central waters (200–700 m) was ENACW of 12°C, which represented 18.1% of the total sampled volume. For the intermediate waters (700–1,500 m), the predominant water mass was AA, with 10.6% of the volume, and for the deep waters (1,500 m–bottom) it was LSW with 15.6% of the volume. Archetype values are used as a mean to simplify the presentation of results that are shown hereinafter.

AOU, a canonical tracer for mineralization processes in the ocean interior, showed maximum values in the Southern and Eastern transects (Figure 4). The highest AOU corresponded to the SACW of 12°C with an overall archetype concentration of 191.7 (5.4) μmol kg^{-1}, mainly located in the Southern and Eastern transects, and the lowest AOU corresponded to the MMW with an archetype concentration of 50.9 (10.5) μmol kg^{-1}, mainly located in the Northern and Western transects. In the intermediate and deep waters, AOU decreased with depth from 175.7 (4.2) μmol kg^{-1} in SPMW to 85.1 (1.7) μmol kg^{-1} in the LNEADW. Water types mixing (Equation 6)

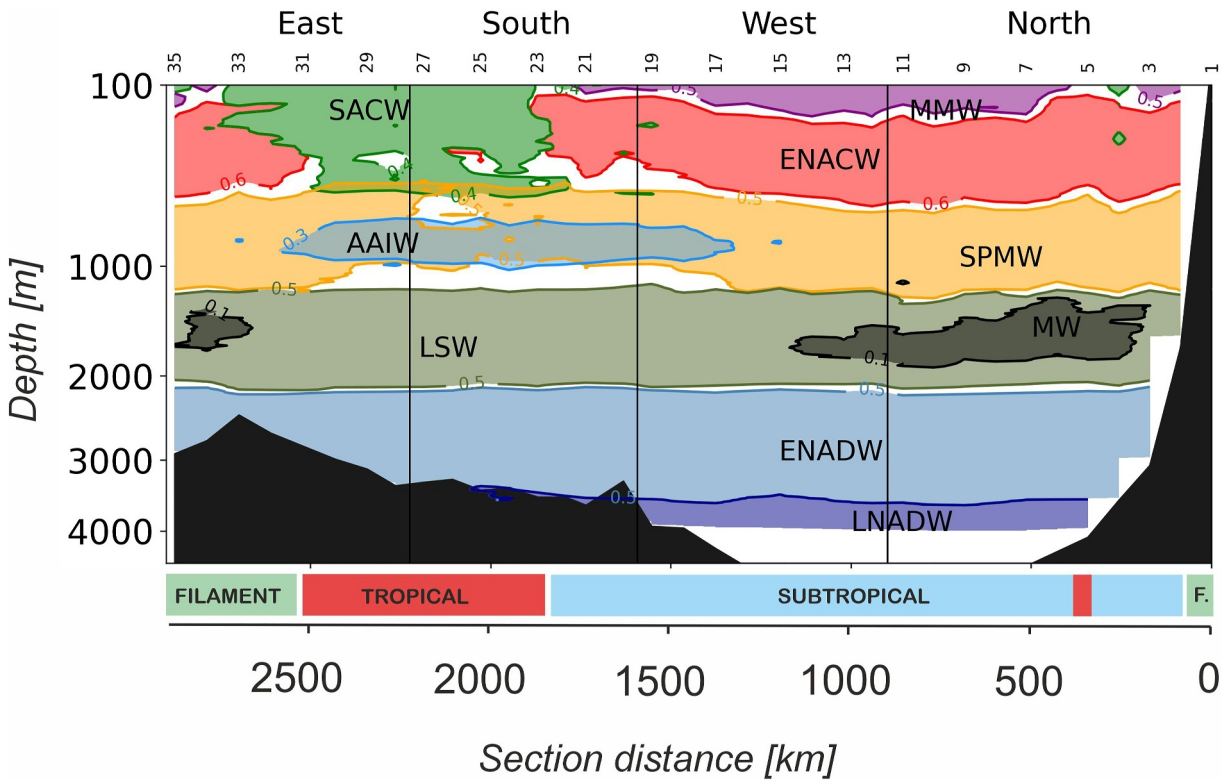

Figure 3. Distribution of water masses in July–August 2017 within the hydrographic box. The dominant water mass is represented at each depth and location. Numbers of isolines indicate the proportion of the water mass. F., Filament.

explained 94% of the variability of AOU in the meso- and bathypelagic waters of the CVFZ, but with a SE of 12.9 μmol kg^{-1}, that is, an order of magnitude higher than the measurement error of about 1 μmol kg^{-1} (Table 2).

The vertical distribution of DOC showed chimney-like columns of high DOC concentration (Figure 4), suggesting a connection between the organic matter produced in shallow levels with the deep waters and/or a lateral advection/interaction between water masses in the mesopelagic layer. These columns of higher DOC are present in all transects. Nevertheless, archetype values showed the typical profile with higher values in shallower waters and a progressive decrease with increasing depth. SACW of 18°C, centered at 102 m, had and archetype concentration of 58.9 (1.9) μmol L^{-1} and the LNEADW, centered at 3,823 m, 42.9 (1.0) μmol L^{-1}. Water type mixing explained 71% of the DOC variability with an SE of 3.4 μmol L^{-1} (Table 2). Compared to AOU, the R^2 is lower, but the SE is only 2-3-fold the measurement error of DOC.

When AOU was added to the multiple linear regression of DOC with X_{ij} (Equation 7), the explained variability increased to 72%. Interestingly, a significant AOU-DOC β coefficient of −0.026 (0.015) mol C mol O_2^{-1} was obtained (Table 3).

3.2. Optical Properties of Colored and Fluorescent DOM in the Epipelagic Layer

$a_{CDOM}(254)$ and $a_{CDOM}(325)$ are among the most commonly used absorption coefficients in marine organic matter biogeochemistry (Álvarez-Salgado et al., 2023). $a_{CDOM}(254)$ is a tracer for conjugated carbon double bonds in DOM and has been suggested as a proxy to the concentration of DOC (Catalá et al., 2018; Lønborg & Álvarez-Salgado, 2014). Moreover, $a_{CDOM}(254)$ is not directly affected by solar radiation since very few solar photons of <295 nm reach the Earth surface (Fichot & Benner, 2012). Conversely, $a_{CDOM}(325)$ is used as a proxy to the aromatic fraction of DOM and a tracer of microbial production and/or photochemical degradation processes due to its sensitivity to solar UV radiation (Iuculano et al., 2019; Nelson et al., 1998, 2004). The ratio $a_{CDOM}(254)/a_{CDOM}(325)$ is an inverse indicator of the CDOM molecular size (Dahlén et al., 1996; Engelhaupt et al., 2003), being lower in freshly produced CDOM (higher molecular size) and increases during microbial and photochemical

21699291, 2025, 7, Downloaded from https://agupubs.onlinelibrary.wiley.com/doi/10.1029/2024JC022068 by Universidad De Las Palmas De Gran Canaria, Wiley Online Library on [01/08/2025]. See the Terms and Conditions (https://onlinelibrary.wiley.com/terms-and-conditions) on Wiley Online Library for rules of use; OA articles are governed by the applicable Creative Commons License

21699291, 2025, 7, Downloaded from https://agupubs.onlinelibrary.wiley.com/doi/10.1029/2024JC022068 by Universidad De Las Palmas De Gran Canaria, Wiley Online Library on [01/08/2025]. See the Terms and Conditions (https://onlinelibrary.wiley.com/terms-and-conditions) on Wiley Online Library for rules of use; OA articles are governed by the applicable Creative Commons License

Table 2
Thermohaline and Chemical Characteristics (Archetype Value ± SE) of Meso- and Bathypelagic Waters

WTs	VOL$_i$ (%)	Z_i (db)	θ_i (ºC)	S_i	Turbidity (10^{-2} NTU)	AOU$_i$ (μmol kg^{-1})	DOC$_i$ (μmol L^{-1})	$a_{CDOM}254_i$ (m^{-1})	$a_{CDOM}325_i$ (m^{-1})
SACW_18	4.8	102 ± 19	17.3 ± 0.5	36.1 ± 0.08	10.9 ± 1.1	120.2 ± 15.4	58.9 ± 1.9	1.14 ± 0.05	0.22 ± 0.02
MMW	5.5	113 ± 13	18.9 ± 0.3	36.6 ± 0.07	10.8 ± 0.03	50.9 ± 10.5	58.7 ± 1.6	1.10 ± 0.04	0.17 ± 0.02
ENACW_15	12.5	240 ± 14	15.2 ± 0.2	36.0 ± 0.04	10.7 ± 0.2	117.8 ± 6.7	52.2 ± 0.8	0.96 ± 0.01	0.17 ± 0.01
SACW_12	7.3	336 ± 28	12.2 ± 0.3	35.5 ± 0.04	10.6 ± 0.2	191.7 ± 5.4	49.9 ± 0.7	0.92 ± 0.01	0.19 ± 0.01
ENACW_12	18.1	442 ± 19	11.6 ± 0.2	35.5 ± 0.03	10.6 ± 0.3	171.2 ± 4.8	48.4 ± 0.5	0.91 ± 0.01	0.17 ± 0.00
SPMW	7.2	809 ± 32	7.8 ± 0.2	35.1 ± 0.02	10.3 ± 0.1	175.7 ± 4.2	44.8 ± 0.6	0.81 ± 0.01	0.15 ± 0.01
AA	10.6	873 ± 54	7.6 ± 0.3	35.1 ± 0.02	10.2 ± 0.2	172.6 ± 5.7	44.9 ± 0.5	0.81 ± 0.01	0.15 ± 0.00
MW	3.1	1,455 ± 118	5.2 ± 0.4	35.0 ± 0.02	10.4 ± 0.3	119.4 ± 9.2	43.1 ± 0.9	0.79 ± 0.01	0.14 ± 0.01
LSW	15.6	1,688 ± 46	4.5 ± 0.1	35.0 ± 0.01	10.4 ± 0.1	104.0 ± 2.6	43.3 ± 0.4	0.76 ± 0.01	0.14 ± 0.00
UNEADW	11.7	2,742 ± 93	3.1 ± 0.1	35.0 ± 0.01	10.4 ± 0.1	88.0 ± 1.1	43.3 ± 0.5	0.83 ± 0.01	0.16 ± 0.01
LNEADW	3.7	3,824 ± 101	2.4 ± 0.0	34.9 ± 0.00	10.3 ± 0.2	85.1 ± 1.7	42.9 ± 1.0	0.82 ± 0.01	0.16 ± 0.01
R^2						0.94	0.71	0.85	0.59
SE						12.9	3.40	0.04	0.02

WTs	*a*254/*a*365	$S_{(275–295)_i}$ (10^{-2})	$S_{(350–400)_i}$ (10^{-2})	S_{Ri}	C1 (10^{-3} RU)	C2 (10^{-3} RU)	C3 (10^{-3} RU)	C4 (10^{-3} RU)	C5 (10^{-3} RU)
SACW_18	10.5 ± 0.8	2.87 ± 0.12	1.19 ± 0.05	2.44 ± 0.11	23.3 ± 1.4	14.9 ± 1.1	5.8 ± 0.5	6.2 ± 1.0	7.4 ± 1.9
MMW	14.4 ± 1.2	3.45 ± 0.14	1.29 ± 0.06	2.69 ± 0.10	18.1 ± 1.8	10.8 ± 1.4	4.2 ± 0.5	6.1 ± 0.9	9.8 ± 1.8
ENACW_15	12.3 ± 0.5	3.01 ± 0.06	1.26 ± 0.05	2.43 ± 0.07	20.1 ± 0.5	13.0 ± 0.4	5.3 ± 0.2	4.4 ± 0.5	7.4 ± 1.4
SACW_12	10.1 ± 0.4	2.51 ± 0.04	1.14 ± 0.03	2.23 ± 0.06	23.7 ± 0.4	14.6 ± 0.3	6.6 ± 0.1	3.6 ± 0.5	5.3 ± 1.3
ENACW_12	11.5 ± 0.4	2.63 ± 0.04	1.29 ± 0.04	2.08 ± 0.04	22.6 ± 0.3	13.8 ± 0.2	6.4 ± 0.1	3.7 ± 0.4	5.8 ± 0.8
SPMW	12.1 ± 0.5	2.46 ± 0.02	1.43 ± 0.07	1.77 ± 0.06	22.7 ± 0.2	13.2 ± 0.2	6.8 ± 0.1	3.0 ± 0.4	5.6 ± 0.9
AA	12.2 ± 0.5	2.48 ± 0.03	1.46 ± 0.06	1.74 ± 0.05	23.2 ± 0.3	13.2 ± 0.2	6.9 ± 0.1	2.6 ± 0.4	4.7 ± 0.9
MW	13.3 ± 1.0	2.60 ± 0.05	1.66 ± 0.12	1.61 ± 0.08	23.1 ± 0.5	13.0 ± 0.3	7.0 ± 0.2	2.4 ± 0.6	4.9 ± 2.0
LSW	12.9 ± 0.4	2.65 ± 0.02	1.62 ± 0.04	1.66 ± 0.03	23.7 ± 0.3	13.2 ± 0.2	7.1 ± 0.1	2.4 ± 0.3	5.5 ± 1.0
UNEADW	12.3 ± 0.4	2.61 ± 0.03	1.59 ± 0.04	1.66 ± 0.04	25.6 ± 0.6	14.1 ± 0.3	7.8 ± 0.2	2.7 ± 0.3	8.2 ± 1.6
LNEADW	12.7 ± 0.7	2.61 ± 0.05	1.74 ± 0.16	1.58 ± 0.09	23.6 ± 0.7	13.8 ± 0.3	7.5 ± 0.2	3.2 ± 0.5	12.2 ± 3.9
R^2					0.63	0.58	0.76	0.27	0.11
SE					0.002	0.001	0.001	0.002	0.006

Note. R^2, proportion of the total variability explained by WT mixing; SE, standard error of the estimate. Components C1, C2, C4 and C5 corresponds with Coble's (1996) peaks A and C, peak M, peak T and peak B, respectively. Component C3 is similar to Stedmon's et al. (2003) peak D.

degradation processes (lower molecular size; Benner & Amon, 2015). Moreover, the spectral slope $S_{275–295}$ and S_R have been suggested as indices for molecular size of DOM, and specifically $S_{275–295}$ for photochemical transformations and S_R for DOM origin (Helms et al., 2008).

The optical properties of DOM varied considerably at the large scale in the epipelagic layer of the CVFZ, with clear differences between the Subtropical and Tropical-filament domains (Figures 5a–5d). Above the pycnocline, higher $a_{CDOM}(254)$ and $a_{CDOM}(325)$ values were found in the Tropical and filament waters domains, respectively (Table 1), and significant differences ($p < 0.0005$) were observed between the Tropical and Subtropical domains. Noticeably, $a_{CDOM}(325)$ presented values more than twice, 0.31 (0.1) and 0.33 (0.1) m^{-1}, in the Tropical and filament domains than in the Subtropical domain, 0.14 (0.02) m^{-1}. Below the pycnocline, $a_{CDOM}(254)$ and $a_{CDOM}(325)$ decreased, but maintained the highest values in the Tropical domain (Table 1; Figures 5a and 5b). At stn 5, the water intrusion from the Tropical domain showed an impact on the CDOM distribution with an increment in the $a_{CDOM}(254)$ and $a_{CDOM}(325)$ values (Figures 5a and 5b). $a_{CDOM}(254)/a_{CDOM}(365)$ presented the

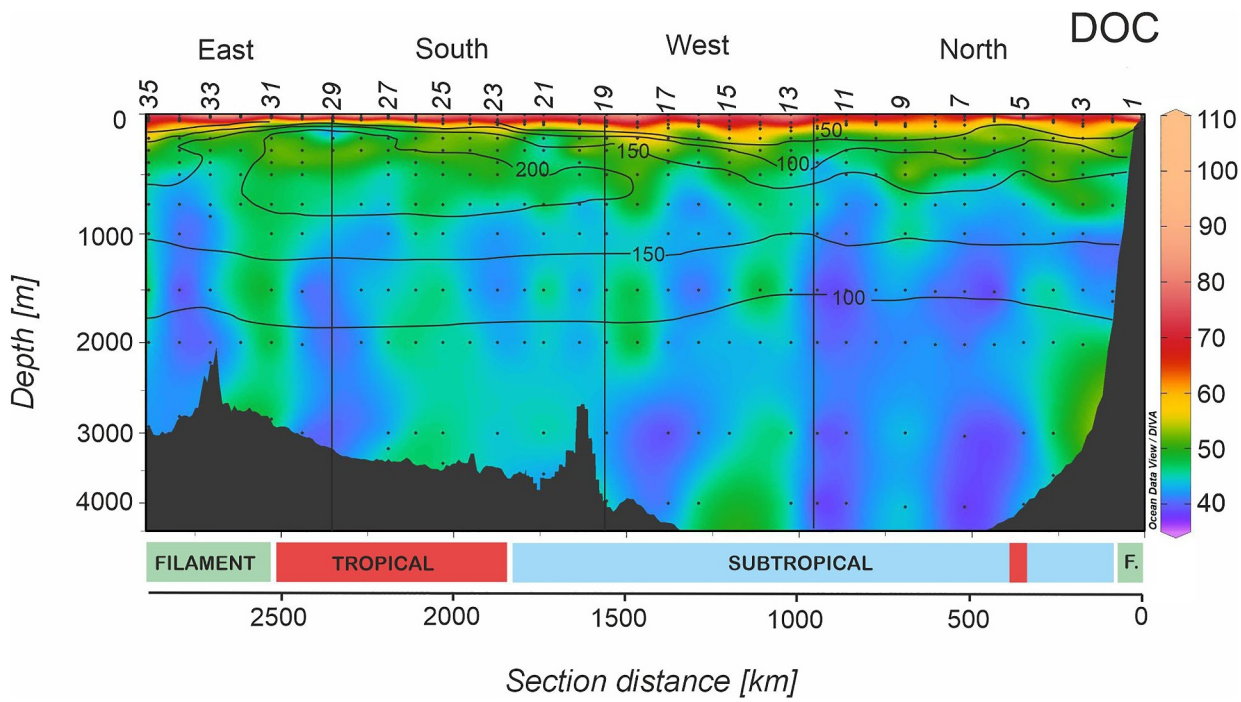

Figure 4. Full depth distribution of dissolved organic carbon in μmol L^{-1} in July-August 2017. Contour lines presents Apparent oxygen utilization in μmol kg^{-1}. Dots represent the sampling depths and vertical black lines represent the corners of the FLUXES I hydrographic box. Note that the *y*-axis (depth) is not linear. F., filament. Odd station numbers are represented at the top of the panel. Produced with Ocean Data View (Schlitzer, 2017).

highest values above the pycnocline and in the Northern and Western transects coinciding with the Subtropical domain (Table 1, Figure 5c). This area matched with the lowest values of $a_{CDOM}(254)$ and $a_{CDOM}(325)$. The slope $S_{275–295}$ was also significantly higher above than below the pycnocline, with the highest values in the Subtropical domain (4.15 (0.03) 10^{-2} nm^{-1}; Table 1, Figure 5d). Similarly, S_R showed the highest values in the Subtropical domain and significantly higher values ($p < 0.0005$) below than above the pycnocline.

Humic-like components C1 to C3 presented parallel distributions, with the highest values being recorded near the coast and centered at the DCM (Table 1, Figures 6a and 6b). Above the pycnocline, values were higher in the filament domain, but below the pycnocline, higher values were observed in the Tropical domain. The correlation between the three humic-like components in the epipelagic layer was higher for C1–C3 ($R^2 = 0.92$) and lower for C1–C2 ($R^2 = 0.81$) and C2–C3 ($R^2 = 0.73$). We do not discuss fluorophore C3 due to its high correlation with C1.

Despite the high correlation between C1 and C2, some differences were observed mainly above the pycnocline, where C1 was higher in the CBGF than in the Tropical domains. Regarding the protein-like components, C4 showed the highest values also in the surface mixed layer near the coast in the Tropical and filament domains. Then decreased with depth to more homogeneous values below the pycnocline, with significantly higher values ($p < 0.0005$) in the Tropical domain as compared with the Subtropical domain (Table 1, Figure 6c). C5 (Figure 6d) showed the highest values above the pycnocline and in the Tropical domain, but contrary to what have been observed for C4, below the pycnocline, higher values were found in the Subtropical domain (Table 1). Moreover, while maximum values of C4 are located at stn 1, 3, 25–33, for C5 are located at stn 11–12, 23–26, indicating therefore a different distribution of these components. Regarding the water intrusion from the Tropical waters at stn 5, it has an impact on the FDOM distribution, presenting higher values mainly of C1, C2 and C4 (Figures 6a–6c).

3.3. Optical Properties of Colored and Fluorescent DOM in the Meso- and Bathypelagic Layers

CDOM at the two chosen wavelengths, $a_{CDOM}(254)$ and $a_{CDOM}(325)$, decreased considerably with depth, from archetype values of 1.14 (0.05) and 0.22 (0.02) m^{-1} in SACW_18 to 0.76 (0.01) and 0.14 (0.01) m^{-1} in LSW, respectively. Noticeably, a significant increase in the bathypelagic water masses was observed, with archetype

21699291, 2025, 7, Downloaded from https://agupubs.onlinelibrary.wiley.com/doi/10.1029/2024JC022068 by Universidad De Las Palmas De Gran Canaria, Wiley Online Library on [01/08/2025]. See the Terms and Conditions (https://onlinelibrary.wiley.com/terms-and-conditions) on Wiley Online Library for rules of use; OA articles are governed by the applicable Creative Commons License

Table 3
Parameters of the Linear Mixing (Equation 6) and Linear Mixing + Biogeochemical (Equation 7) Models

N_1	N_2	R^2	SE	β	SE (β)	p	n
AOU		0.94	12.9				307
DOC		0.71	3.40				302
DOC	AOU	0.72	3.42	−0.026	0.015	0.05	302
$a_{CDOM}254$		0.85	0.04				236
$a_{CDOM}325$		0.59	0.02				236
$a_{CDOM}254$	AOU	0.85	0.04	–	–	–	236
$a_{CDOM}325$	AOU	0.60	0.02	–	–	–	236
C1		0.63	0.002				217
C2		0.58	0.001				217
C3		0.76	0.001				217
C4		0.27	0.002				210
C5		0.11	0.006				211
C1	AOU	0.64	0.002	$2.3\ 10^{-5}$	$9.1\ 10^{-6}$	0.01	217
C2	AOU	0.63	0.001	$2.5\ 10^{-5}$	$5.2\ 10^{-6}$	$2.3\ 10^{-6}$	217
C3	AOU	0.76	0.001	–	–	–	217
C4	AOU	0.29	0.002	$-2.23\ 10^{-5}$	$9.81\ 10^{-6}$	0.02	210
C5	AOU	0.12	0.006	–	–	–	211

Note. R^2, determination coefficient; SE, standard error of the estimate; β, fitting parameter of the relationship between N1 and N2 independent of the mixing; SE (β), standard error of the estimation of β; *p*, significance level of the estimation of β; *n*, number of samples. Hyphens correspond with non-significant observations.

values of 0.82 (0.01) and 0.16 (0.01) m^{-1} in LNEADW, not accompanied by parallel increases in DOC nor AOU. This increment was most noticeable in the Eastern transect, followed by the Northern transect as can be observed in the CDOM sections of Figures 5a and 5b and Table S3 in Supporting Information S1, mainly associated to the Mauritanian continental slope. $a_{CDOM}(254)$ and $a_{CDOM}(325)$ showed high differences between transects, with the lowest values below 1,000 m in the stations farthest from the coast, from stn 7 to stn 25. The $a_{CDOM}(254)/a_{CDOM}(365)$ ratio, a proxy for the average molecular weight of CDOM, showed higher archetype values in the Northern and Western transects with a maximum of 15.8 (2.0) in the MMW (Table S3 in Supporting Information S1), than in the Southern and Eastern transects. Particularly, the Eastern transect presented the lowest values, with a minimum of 8.7 (0.6) in the SACW_18. From stn 7 to stn 25, an area of relatively high $a_{CDOM}(254)/a_{CDOM}(365)$ (~20) was observed from 1,000 m to bottom, compared to their surroundings (~10). In this area, an increase of the spectral slope $S_{275–295}$ (Figure 5d) and a decrease of S_R (not shown) were also observed.

Fluorophores C1 and C2 matched the distribution of CDOM, with the highest values in shallower waters at the Eastern and Southern transects (stn 25–35) and a remarkable increase in the near-bottom waters of the same transects (Figures 6a and 6b). Maximum values of C1 were observed in the two NEADW water types at the Eastern transect with an average of 30.1 (1.8) and 32.1 (2.4) 10^{-3} RU, which were significantly higher ($p < 0.005$) than in the Western transect (Table S3 in Supporting Information S1). C1 and C2 were also significantly higher ($p < 0.005$) in the Southern than in the Northern transects for the SACW of 12 and 18°C but showed similar values in both transects for ENACW. For the intermediate waters, differences were found between SPMW and AA, being higher again in the Southern transect for C1, but similar for C2.

Regarding the protein-like C4 (Figure 6c), it generally decreased with depth from central to intermediate waters. Then, it presented similar archetype values for intermediate and deep waters (Table 2). The highest archetype values were observed in the Northern transect for SACW of 18°C and MMW with values of 7.7 (3.2) and 7.0 (2.3) 10^{-3} RU, and the lowest in the Eastern one for SPMW and LSW with 1.8 (0.8) and 1.8 (0.4) 10^{-3} RU (Table S3 in Supporting Information S1). Finally, C5 (Figure 6d) showed similar archetype values in the central and intermediate waters, with a significant increase in deep waters in the Northern and Southern transects. Nevertheless, this increase was not observable in the Eastern transect, which contained the lowest values of this component (2.6 (1.6) 10^{-3} RU for the LNEADW, Table S3 in Supporting Information S1).

The distribution of particles (turbidity; Figure 7) is also presented to check for similarities with the distributions of CDOM and FDOM parameters. Turbidity shows columns of higher particle density that distributes from surface to bottom in the Eastern and Northern transects, being more intense in the former; significantly ($p < 0.005$) higher values were obtained for the Eastern transect although not for all the water masses (Table S3 in Supporting Information S1). In Figure 7, the largest nepheloid layer occurs in surface waters close to the coast, from stn 1–7 and 26–35, coinciding with higher values of $a_{CDOM}(254)$, $a_{CDOM}(325)$, C1, C2 and C3 mainly at the second group of stations. It is related to the biomass accumulation due to the high primary production of the area (Gabric et al., 1993).

Water type proportions (X_{ij}) (Equation 6) explained 85% and 59% of the $a_{CDOM}(254)$ and $a_{CDOM}(325)$ variability with an SE of 0.04 and 0.02 m^{-1}, respectively (Table 3). For comparison, the measurement error is 0.02 m^{-1}, that is of the same order than the SE. When AOU is added to the model, no increase was observed in the explained variability and the $a_{CDOM}(254)$-AOU and $a_{CDOM}(325)$-AOU β coefficients were not significant. Regarding the fluorescent fraction of DOM, water mass mixing explained 63%, 58%, 27% and 11% of the C1, C2, C4 and C5 components, with SE of 2, 1, 2 and 6 10^{-3} RU, respectively. The corresponding measurement errors of C1, C2, C4 and C5 are 0.5, 0.3, 0.2 and 0.4 10^{-3} RU, respectively, that is, about an order of magnitude lower than the

21699291, 2025, 7, Downloaded from https://agupubs.onlinelibrary.wiley.com/doi/10.1029/2024JC022068 by Universidad De Las Palmas De Gran Canaria, Wiley Online Library on [01/08/2025]. See the Terms and Conditions (https://onlinelibrary.wiley.com/terms-and-conditions) on Wiley Online Library for rules of use; OA articles are governed by the applicable Creative Commons License

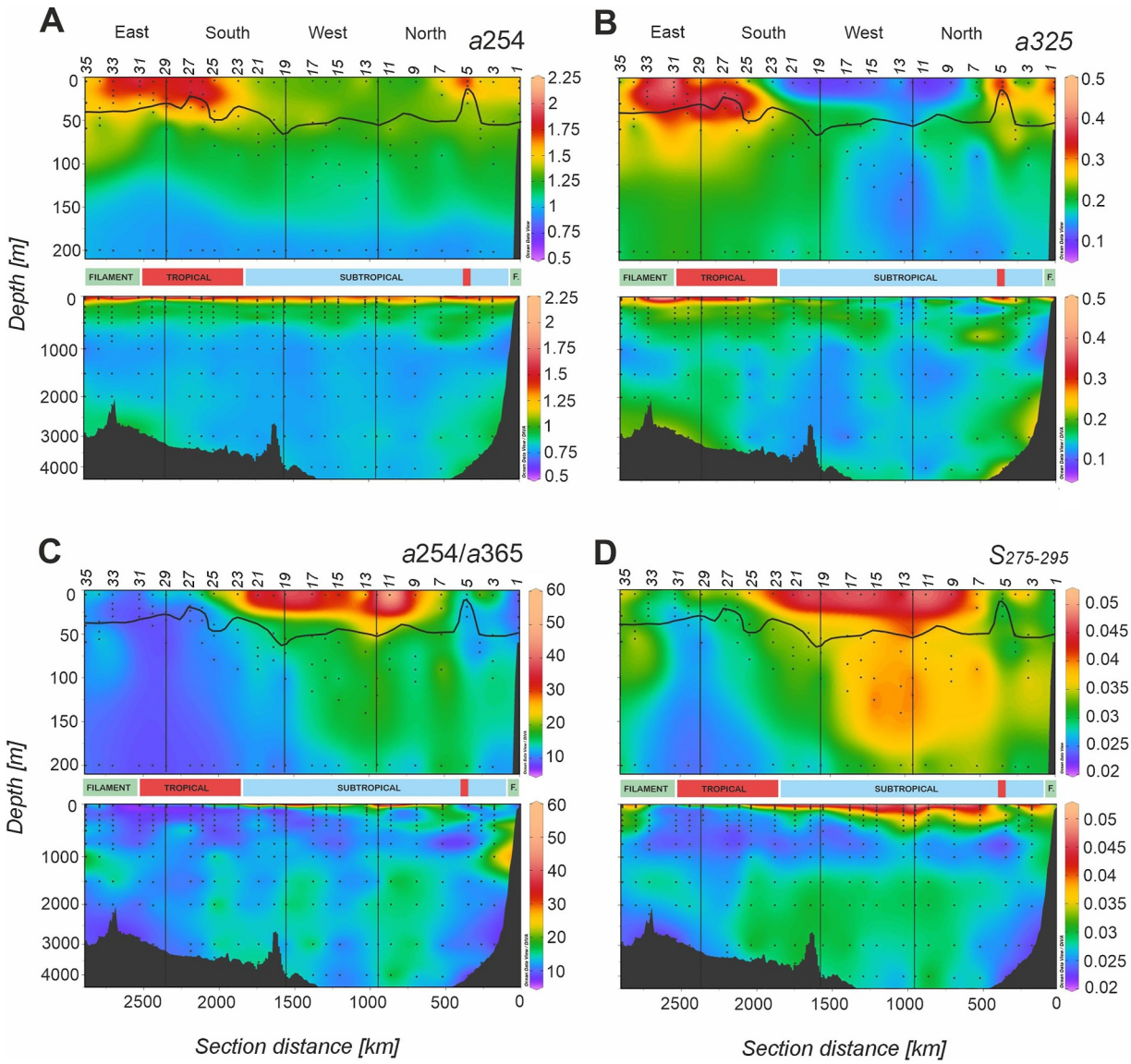

Figure 5. Distributions of (a) absorption coefficient at 254 nm ($a_{CDOM}254$) in m^{-1}, (b) absorption coefficient at 325 nm ($a_{CDOM}325$) in m^{-1}, (c) ratio of absorption coefficients $a_{CDOM}254/a_{CDOM}365$ and (d) spectral slope $S_{275-295}$ in nm^{-1} in July-August 2017. Dots represent the sampling depths, horizontal black line show the position of the pycnocline and the vertical black lines represent the corners of the FLUXES hydrographic box. F., filament. Odd station numbers are represented at the top of the first panel. Produced with Ocean Data View (Schlitzer, 2017).

corresponding SE (Table 3). When AOU is added to the multiple regression model (Equation 7), the explained variability increased to 64%, 63%, 29% and 12%. The C1-AOU, C2-AOU and C4-AOU β coefficients were significant, with values of 2.3 (0.9) 10^{-5}, 2.5 (0.5) 10^{-5} and −2.2 (1.0) 10^{-5} RU kg^{-1} µmol (Table 3). On the contrary, the protein-like fluorophore C5 did not have a significant β coefficient with AOU.

4. Discussion

4.1. New Insights on DOM Cycling in Epipelagic Waters of the CVFZ

The interplay of the CVF and the CBGF led to the classification of the epipelagic layer into three domains: subtropical, tropical and filament. The tropical domain was fertilized by the nutrient-rich SACW and was characterized by a shallower and more stable pycnocline, and higher Chl-*a* concentrations. These hydrographic conditions explain the observed accumulation of DOC and the colored and fluorescent fractions DOM in the tropical domain associated with a relatively higher primary production above the pycnocline and reduced

21699291, 2025, 7, Downloaded from https://agupubs.onlinelibrary.wiley.com/doi/10.1029/2024JC022068 by Universidad De Las Palmas De Gran Canaria, Wiley Online Library on [01/08/2025]. See the Terms and Conditions (https://onlinelibrary.wiley.com/terms-and-conditions) on Wiley Online Library for rules of use; OA articles are governed by the applicable Creative Commons License

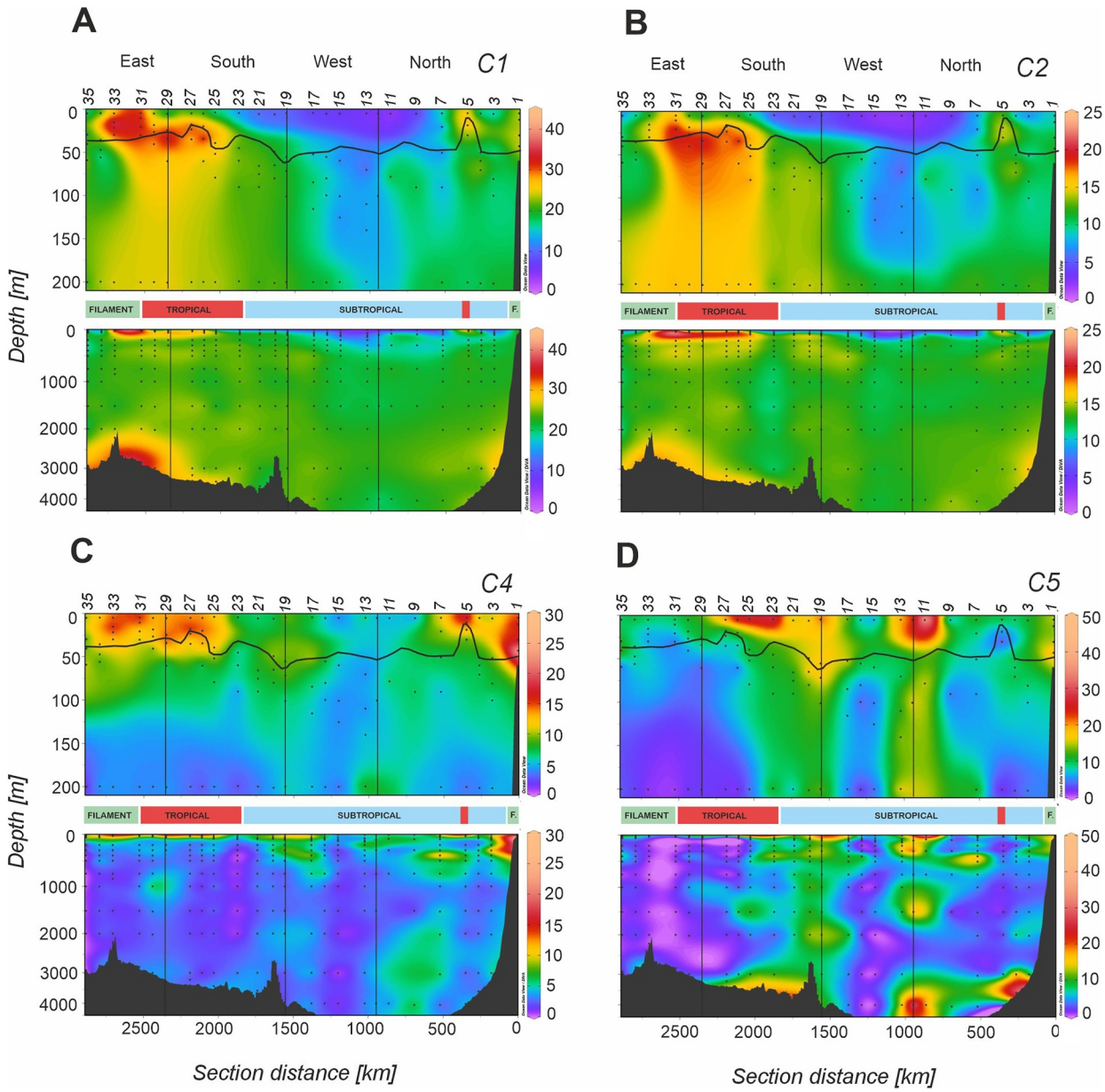

Figure 6. Distributions of (a) fluorescence component C1 in 10^{-3} RU, (b) fluorescence component C2 in 10^{-3} RU, (c) fluorescence component C4 in 10^{-3} RU and (d) fluorescence component C5 in 10^{-3} RU in July-August 2017. Dots represent the sampling depths, horizontal black line show the position of the pycnocline and the vertical black lines represent the corners of the FLUXES hydrographic box. F., filament. Odd station numbers are represented at the top of the first panel. Produced with Ocean Data View (Schlitzer, 2017).

exchange with the waters below the pycnocline due to a higher stratification. On the contrary, CDOM and FDOM signals were lower in the subtropical domain, where biological activity was lower and therefore, indirectly leads to lower levels of organic matter production and processing. Moreover, the persistent photodegradation favor the bleaching of the accumulated materials (Helms et al., 2008; Lønborg et al., 2015). As a result, minimum values of $a_{CDOM}(325)$ and maximum values of the $a_{CDOM}(254)/a_{CDOM}(325)$ ratio and the slope $S_{275-295}$, characteristic of intense photooxidation processes (Del Vecchio & Blough, 2004; Helms et al., 2008; Siegel et al., 2005; Swan et al., 2012), were observed. Waters in the subtropical domain are transported southwestward by the Canary Current (see Figure 1; Pelegrí & Peña-Izquierdo, 2015a), away from the influence of the upwelling system and therefore, are not expected to receive inputs of fresh DOM. The $a_{CDOM}(254)/a_{CDOM}(365)$ ratio is lower in the filament waters, indicating a larger molecular size of DOM in that domain, as expected due to the export of

21699291, 2025, 7, Downloaded from https://agupubs.onlinelibrary.wiley.com/doi/10.1029/2024JC022068 by Universidad De Las Palmas De Gran Canaria, Wiley Online Library on [01/08/2025]. See the Terms and Conditions (https://onlinelibrary.wiley.com/terms-and-conditions) on Wiley Online Library for rules of use; OA articles are governed by the applicable Creative Commons License

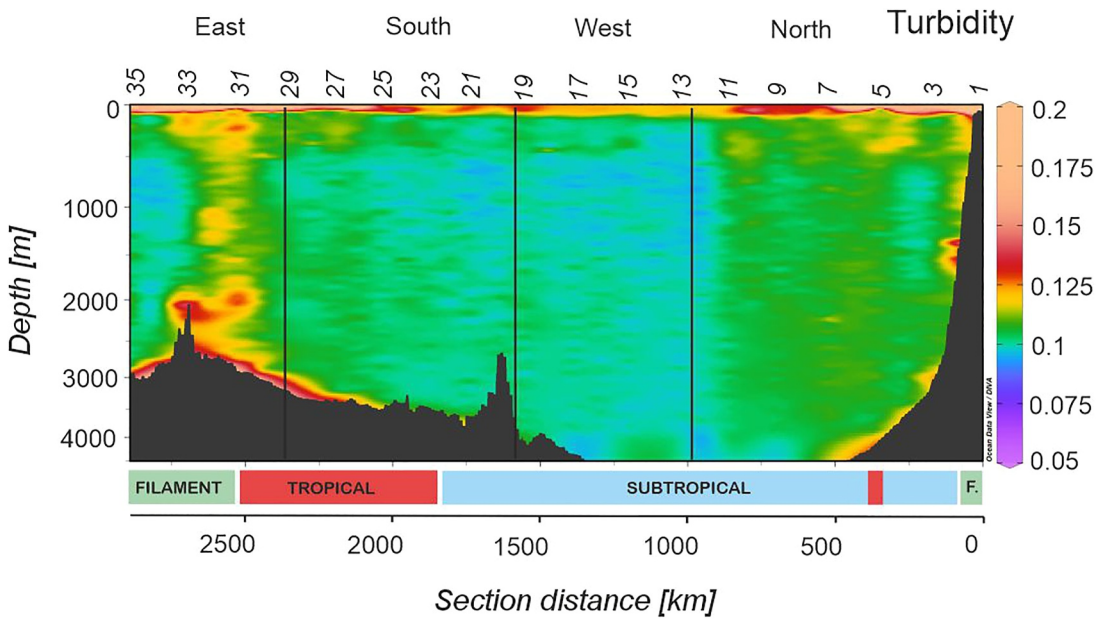

Figure 7. Full depth distribution of turbidity in Nephelometric Turbidity Units (NTU) in July–August 2017. Vertical black lines represent the corners of the FLUXES I hydrographic box. Note that the *y*-axis (depth) is not linear. F., filament. Odd station numbers are represented at the top of the first panel. Produced with Ocean Data View (Schlitzer, 2017).

recently-formed bioavailable organic matter from the Mauritanian upwelling. This is consistent with the size-reactivity continuum hypothesis, which states that recently-formed organic matter with a larger molecular size is on average more reactive than reworked and lower molecular weight organic matter (Benner & Amon, 2015). Moreover, this recently upwelled water has not experienced significant photochemical degradation. The spectral slope $S_{275–295}$ corroborated higher photochemical degradation of DOM in the subtropical domain, mainly above the pycnocline of the Northern and Western transects. Finally, S_R showed values >2, indicative of the dominant marine origin of the DOM in the CVFZ (Helms et al., 2008).

Fluorophores C1 and C3, which highly correlated, correspond to humic and fulvic acids of terrestrial origin, respectively, while fluorophore C2 correspond to marine humic-like substances (Coble, 1996; Stedmon et al., 2003). These fluorophores followed the same distribution pattern than CDOM absorption coefficients. Higher values were found at the Eastern and the easternmost end of the Southern transects due to its proximity to the coast, where higher rates of primary production would led to higher microbial respiration rates and the resultant accumulation of the marine humic-like fluorophore C2 (Catalá et al., 2016; Nieto-Cid et al., 2006; Yamashita & Tanoue, 2008). The terrestrial humic-like florophores C1 and C3 are transported to the coast via continental runoff, for example from the Senegal River (Mbaye et al., 2016) or atmospheric deposition, for example Sahara dust (Arístegui et al., 2009; Campanero et al., 2022). It has been recently shown that Sahara dust contains elevated concentrations of highly reworked humic-like DOM, which suggests that terrestrial humic-like substances increase their concentration in the water column after Sahara dust deposition (Campanero et al., 2022). Alternatively, iron oxides present in the Sahara dust and its dissolution in the water column also enhances the absorption and fluorescence properties of DOM (Linke et al., 2006; Xiao et al., 2013). This could explain the observed differences in the distribution of C1 and C2 in the surface mixed layer of the filament domain, where higher fluorescence intensities of C1 were observed.

The protein-like fluorophores C4 and C5 showed a clear decline below the pycnocline likely due to the labile nature of these materials, which are rapidly consumed by heterotrophic organisms (Jørgensen et al., 2011; Stedmon & Markager, 2005a, 2005b). C4 showed maximum values at the Eastern transect and the Northern and Southern transects near the coast, as expected since fresh DOM is produced in the coastal upwelling system and exported by the CBGF (Gabric et al., 1993). Moreover, when comparing C4 with DOC, we observed that a relatively higher signal of C4 was present in the filament domain, as expected due to the high primary production rates, subsequent production of labile DOM as fluorophore C4 and offshore export by the CBGF.

21699291, 2025, 7, Downloaded from https://agupubs.onlinelibrary.wiley.com/doi/10.1029/2024JC022068 by Universidad De Las Palmas De Gran Canaria, Wiley Online Library on [01/08/2025]. See the Terms and Conditions (https://onlinelibrary.wiley.com/terms-and-conditions) on Wiley Online Library for rules of use; OA articles are governed by the applicable Creative Commons License

4.2. New Insights on DOM Cycling in Meso- and Bathypelagic Waters of the CVFZ

Organic matter distributions in the meso- and bathypelagic layers of the CVFZ were driven by the surface dynamics, where most of the organic matter is produced in situ by primary producers or exported from the shelf by the CBGF (Gabric et al., 1993; Meunier et al., 2012). A quick connection between the surface and the deep ocean was observed, mostly in the eastern transect due to its proximity to the coast. The distribution of turbidity (Figure 7), a proxy to particle concentration (Cetinić et al., 2012), suggest larger concentrations of sinking particulate organic matter near the coast, and in the columns of higher DOC reaching deep waters (Figure 4). Previous studies in the region of Cape Blanc reported this surface-to-deep connection, related to the ballasting effect of lithogenic material produced in situ or from atmospheric inputs associated to processes of absorption-desorption of DOM onto particles (Bory & Newton, 2000; Campanero et al., 2022; Fischer et al., 2016; Fischer & Karakaş, 2009; Valiente et al., 2022; van der Jagt et al., 2018). The DOC distribution in columns could be related to the episodic and likely patchy deposition of Saharan dust in the area (Matzenbacher et al., 2024). When natural plankton communities are exposed to Saharan dust deposition, higher abundance of aggregates with faster sinking velocities compared to aggregate formation with low dust are observed (van der Jagt et al., 2018). Furthermore, the process of partial dissolution of sinking particles to produce DOM has been previously observed (Simon et al., 2002; Smith et al., 1992), and also the connection between the surface layer and the deep ocean in other regions (Gómez-Letona et al., 2022; Lopez et al., 2020; Ruiz-González et al., 2020).

Nepheloid layers at intermediate (intermediate nepheloid layer, INL) and bottom depths (bottom nepheloid layer, BNL) are commonly observed in this study area (Fischer et al., 2009, 2019; Karakaş et al., 2006; McCave, 1986). In the FLUXES I cruise no clear INL was found, instead a column of relatively homogeneous and elevated turbidity was observed through the mesopelagic layer, connecting epipelagic and bathypelagic waters (Figure 7). Finally, in the bathypelagic layer, a BNL was found with higher values at the Eastern transect between stn 29–35 and at the Northern transect between stn 1–7. This BNL is coincident with the high bottom values of $a_{CDOM}(254)$, $a_{CDOM}(325)$, C1, C2 and C3 at the same groups of stations.

These distributions at the BNL could be caused by the release of CDOM and FDOM contained in particles sinking from the epipelagic layer, ballasted with Sahara dust, which connect the surface production with the BNL. As already indicated, Sahara dust contains humic-like FDOM that is released to the water column (Campanero et al., 2022). In this regard, fluorescence intensity of C1 is higher than C2 in the BNL, which is consistent with a terrestrial origin of this fluorescence signal. In addition, iron oxides in the Sahara dust may also enhance the absorption and fluorescence properties of DOM (Linke et al., 2006; Xiao et al., 2013). Moreover, humic-like fluorescence can also be produced during the degradation of organic matter in sinking particles, being released when the particles reach the bottom, explaining the maximum of C2, with marine origin. Independently of the origin of the humic-like fluorescence maxima, release from Sahara dust or degradation of sinking particles in mesopelagic waters, no increase of AOU in the BNL as observed, should be expected. Important fluxes of fast sinking organic particles and the presence of a well-developed BNL have been consistently reported in the CVFZ (Fischer et al., 2009, 2019; Karakaş et al., 2006; Ohde et al., 2015). Fischer et al. (2009) showed a BNL in the Cape Blanc region that slid along the bottom slope comprising particles with settling rates >30 m d^{-1}. This BNL extended up to over 1,000 m above the seafloor with some seasonal variability. Alternatively, the fluorescence humic-like maxima in the BNL could be related with the resuspension of reworked organic matter accumulated in anoxic sediments, as was documented in the Arctic ocean (Chen et al., 2016), Sea of Japan (Kim & Kim, 2016) and the eastern tropical South Pacific (Loginova et al., 2020). The distribution of the tryptophan-like component C4 did not match the areas of higher particle density in the meso- and bathypelagic layers, likely due to a rapid degradation of these materials (Jørgensen et al., 2011). Conversely, the distribution of C5 is patchy, presenting high values in the meso- and bathypelagic layers. Since C5 could be a mixture between tyrosine-like and PAHs, no clear spatial pattern would be expected. This patchy distribution has been already observed all along the Atlantic Ocean by Jørgensen et al. (2011), arguing that higher values of protein-like materials at higher depths could be explained by the drawdown of these materials during deep North Atlantic water mass formation, along with a higher refractory nature of tyrosine-like than tryptophan-like substances (Stedmon & Markager, 2005a, 2005b).

The multiple linear regression of DOC and POC with water mass proportions (X_{ij}) in the FLUXES I hydrographic box, and the addition of AOU to each variable in the multiple regression model have been previously analyzed by Valiente et al. (2022). They observed that only a small fraction of DOC (3.6 ± 2.1%) and suspended POC

21699291, 2025, 7, Downloaded from https://agupubs.onlinelibrary.wiley.com/doi/10.1029/2024JC022068 by Universidad De Las Palmas De Gran Canaria, Wiley Online Library on [01/08/2025]. See the Terms and Conditions (https://onlinelibrary.wiley.com/terms-and-conditions) on Wiley Online Library for rules of use; OA articles are governed by the applicable Creative Commons License

21699291, 2025, 7, Downloaded from https://agupubs.onlinelibrary.wiley.com/doi/10.1029/2024JC022068 by Universidad De Las Palmas De Gran Canaria, Wiley Online Library on [01/08/2025]. See the Terms and Conditions (https://onlinelibrary.wiley.com/terms-and-conditions) on Wiley Online Library for rules of use; OA articles are governed by the applicable Creative Commons License

(4.5 ± 0.7%) contributed to the production of inorganic carbon in the area covered by the hydrographic box (assuming a $-O_2$:C Redfield ratio of 1.4 mol O_2 mol C^{-1} (Anderson, 1995)), concluding that the main responsible for the remaining (92%) remineralized organic carbon was the sinking fraction. In our study, the optical properties of DOM were analyzed, and the multiple linear regression model showed that water mass mixing explained better $a_{CDOM}(254)$ (85%) than $a_{CDOM}(325)$ (59%). This pattern was also observed in previous studies in the eastern North Atlantic (Campanero et al., 2022; Lønborg & Álvarez-Salgado, 2014) and in the Mediterranean Sea (Catalá et al., 2018) and it is related to the exponential decay of the absorption coefficient with increasing wavelength, which produces higher relative measurement errors at longer wavelengths. In general, a large measurement error tends to produce both lower R^2 and lower ratios between the standard error of the estimate (SE) provided by the mixing model and the measurement error. When AOU was added to the model, no significant β coefficients were obtained for $a_{CDOM}(254)$ and $a_{CDOM}(325)$, indicating that local-scale mesopelagic mineralization processes did not affect significantly these DOM fractions in the CVFZ. Note that the residence time of mesopelagic waters in the hydrographic box has been calculated at around 60 days (Burgoa et al., 2021), which is too short to produce a significant and observable local signal of the degradation of the recalcitrant (mainly semilabile and semi-refractory) fraction of DOM, that requires longer periods of time to be processed, from 1.5 to 20 years, respectively (Hansell, 2013). Furthermore, the fact that the SE of the linear regressions with X_{ij} are of the same order of the measurement error, may indicate that the analytical method is not accurate enough to catch these subtle local processes in such a short time scale.

Regarding the FDOM fraction, fluorophores C1 and C2 presented higher values of explained variability due to the water masses mixing (63% and 58%, respectively), contrary to the lower values observed for C4 and C5 (27% and 11%, respectively), related to protein-like materials. Nevertheless, the SE of the FDOM components were an order of magnitude higher than the measurement error, indicating that basin-scale processes alone cannot explain the observed distribution in the ocean interior despite the relatively high R^2 (Álvarez-Salgado et al., 2013). Fluorophores C1 and C2 increased the explained variability when AOU was added to the model (64% and 63%, respectively), with significant positive β coefficients suggesting the local accumulation of refractory materials in parallel to DO consumption in the CVFZ. Therefore, contrary to CDOM, FDOM measurements are sensitive enough to detect the subtle local-scale accumulation that occurs in mesopelagic waters of the CVFZ. This accumulation of humic-like substances in the dark ocean is presumably related with the microbial carbon pump mechanism (Jiao et al., 2010). Moreover, the recent study by Xiao et al. (2023) proposed to use the relationship between FDOM and AOU as an indicator for evaluating the microbial carbon pump efficiency in the dark ocean. In this regard, the obtained β coefficients of 2.3 (0.9) and 2.5 (0.5) 10^{-5} RU kg^{-1} µmol for C1 and C2 are comparable to those obtained in previous observations made also in the CVFZ by Campanero et al. (2022, p. 1.8 (0.7) 10^{-5} RU kg^{-1} µmol), in the Mediterranean Sea by Martínez-Pérez et al. (2019; 2.1 (0.4) 10^{-5} RU kg^{-1} µmol) and in the global ocean by Catalá et al. (2015) and Jørgensen et al. (2011) with β coefficients of 2.2 and 2.7 10^{-5} RU kg^{-1} µmol, respectively. Since DOC and suspended POC make a very small contribution to the local DO demand, it has been postulated that the main contributor to the local mineralization of organic matter is the sinking particles with fast settling rates (Valiente et al., 2022). This idea would be consistent with the production of humic-like substances in the dark ocean of the CVFZ from these sinking particles.

Finally, the variability of C4 explained by the water mass mixing model also increased when AOU was added to the model, but contrary to C1 and C2, the β coefficient was negative (−2.2 (1.0) 10^{-5} RU kg^{-1} µmol) indicating net consumption of protein-like materials in the dark ocean of the CVFZ and therefore, revealing their labile nature. This value is comparable to that obtained in the Mediterranean Sea by Martínez-Pérez et al. (2019) for peak T, with a peak T-AOU β coefficient of −3.7 (1.3) 10^{-5} RU kg^{-1} µmol.

5. Conclusions

The distribution of the optically active fraction of DOM in epipelagic waters of the CVFZ allowed us to gain insights on the composition (e.g., molecular weight, origin, bioavailability) and photochemical/microbial processing experienced by DOC in the different domains created by the CVF and the CBGF. Tropical waters south of the CVF and CBGF waters were characterized by high nutrient concentrations and a shallower pycnocline, enabling the accumulation of Chl-*a* and therefore of colored and fluorescent DOM fractions. DOM in the filament waters presented the highest average molecular weight, as expected because of the export of recently formed organic matter from the Mauritanian upwelling. Photochemical degradation of DOM could be particularly intense

at the oligotrophic stations occupied by subtropical waters to the north of the CVF, probably explained by a longer exposure time.

In mesopelagic waters, the separation of local- from large-scale variability of the optically active fractions of DOM, allowed to focus on the local-scale variability of the fluorescent humic- and protein like substances. A positive relationship was observed between components C1 and C2 with AOU, suggesting an accumulation of humic-like compounds in parallel to DO consumption. Conversely, component C4 correlated negatively with AOU, suggesting local consumption due to its labile nature. Therefore, while the relationship between DOC and AOU could just inform us about the contribution of DOC to the DO demand of the mesopelagic layer, the relationship of the fluorescent fraction of DOM with AOU could provide insights on the consumption of labile DOC and the parallel production of refractory DOC. Nevertheless, experimental data would be necessary to fully support these statements.

The bathypelagic waters of the CVFZ are characterized by a well-developed BNL along the continental slope where the colored and fluorescent humic-like fractions of DOM accumulate without a parallel increase in AOU. We hypothesized that DOM release from sinking particles, either of allochthonous (ballasting Sahara dust, containing both FDOM and iron oxides) or autochthonous (organic mineralization of particles) origin and/or the resuspension of reworked organic matter accumulated in anoxic sediments could be the likely reasons for this signal.

List of Acronyms

AA:	Antarctic intermediate water
AABW:	Antarctic bottom water
AOU:	Apparent oxygen utilization
BNL:	Bottom nepheloid layer
CBGF:	Cape blanc giant filament
CC:	Canary current
CDOM:	Colored dissolved organic matter
Chl-*a*:	Chlorophyll-*a*
CUC:	Canary upwelling current
CVF:	Cape Verde front
CVFZ:	Cape Verde Frontal Zone
DCM:	Deep chlorophyll maximum
DO:	Dissolved oxygen
DOC:	Dissolved organic carbon
DOM:	Dissolved organic matter
EEM:	Excitation-emission matrices
Em:	Emission
ENACW:	Eastern North Atlantic Central Water
Ex:	Excitation
FDOM:	Fluorescent dissolved organic matter
INL:	Intermediate nepheloid layer
LNEADW:	Lower North East Atlantic Deep Water

21699291, 2025, 7, Downloaded from https://agupubs.onlinelibrary.wiley.com/doi/10.1029/2024JC022068 by Universidad De Las Palmas De Gran Canaria, Wiley Online Library on [01/08/2025]. See the Terms and Conditions (https://onlinelibrary.wiley.com/terms-and-conditions) on Wiley Online Library for rules of use; OA articles are governed by the applicable Creative Commons License

LSW:	Labrador sea water
MC:	Mauritanian current
MMW:	Madeira modal water
MW:	Mediterranean water
NACW:	North Atlantic Central Water
NEADW:	North East Atlantic Deep Water
NEC:	North equatorial current
nm:	nanometer
OMP:	Optimum multiparameter
PAHs:	Polycyclic aromatic hydrocarbons.
PARAFAC:	Parallel factor analysis
POC:	Particulate organic carbon
PUC:	Poleward undercurrent
RU:	Raman units
S:	Salinity
SACW:	South Atlantic Central Water
SE:	Standard error
SPMW:	Subpolar mode water
TOC:	Total organic carbon
UNEADW:	Upper North East Atlantic Deep Water
WT:	Water type
Z:	depth
θ:	Potential temperature

Conflict of Interest

The authors declare no conflicts of interest relevant to this study.

Data Availability Statement

The raw data supporting the conclusions of this article will be made available by the authors, at Zenodo repository (https://doi.org/10.5281/zenodo.15203464).

References

Álvarez-Salgado, X. A., Álvarez, M., Brea, S., Mèmery, L., & Messias, M. J. (2014). Mineralization of biogenic materials in the water masses of the South Atlantic Ocean. II: Stoichiometric ratios and mineralization rates. *Progress in Oceanography*, *123*, 24–37. https://doi.org/10.1016/J.POCEAN.2013.12.009

Álvarez-Salgado, X. A., Nieto-Cid, M., Álvarez, M., Pérez, F. F., Morin, P., & Mercier, H. (2013). New insights on the mineralization of dissolved organic matter in central, intermediate, and deep water masses of the northeast North Atlantic. *Limnology & Oceanography*, *58*(2), 681–696. https://doi.org/10.4319/LO.2013.58.2.0681

Álvarez-Salgado, X. A., Nieto-Cid, M., & Rossel, P. E. (2023). Dissolved organic matter. In J. Blasco & A. Tovar-Sánchez (Eds.), *Marine analytical chemistry* (pp. 39–102). Springer. https://doi.org/10.1007/978-3-031-14486-8_2

Anderson, L. A. (1995). On the hydrogen and oxygen content of marine phytoplankton. *Deep Sea Research Part I: Oceanographic Research Papers*, *42*(9), 1675–1680. https://doi.org/10.1016/0967-0637(95)00072-E

Acknowledgments

We thank the captain and crew of R/V Sarmiento de Gamboa and the technicians of CSIC Unidad de Tecnología Marina (UTM) for their valuable help during the FLUXES I cruise. This work was funded by MICIU/AEI/10.13039/501100011033 research Grants FLUXES (CTM2015-69392-C3) and e-IMPACT (PID2019-109084RB-C2). R.C.N was supported by a PhD fellowship from the Spanish Ministry of Science and Innovation (BES-2016-076462); B.F.C was supported by a Juan de La Cierva Formación fellowship (FJCI-641-2015-25712) and by the European Union's Horizon 2020 research and innovation program under the Marie Skłodowska-Curie grant agreement No. 834330 (SO-CUP). M.N.-C. was partially supported by the project FERMIO (MINECO, CTM2014–57334–JIN), co-financed with FEDER funds. J.A and X.A. A.S were partly supported by the project OceanICU (HORIZON-CL6-2022-CLIMATE-01-02; 101083922). This manuscript has benefited from discussions with members of the SCOR working groups 155 (Eastern boundary upwelling systems (EBUS): diversity, coupled dynamics and sensitivity to climate change) and 161 (Respiration in Mesopelagic Ocean, REMO). We also thank the reviewers for helpful comments that improved the original draft and the associate editor for handling the manuscript.

21699291, 2025, 7, Downloaded from https://agupubs.onlinelibrary.wiley.com/doi/10.1029/2024JC022068 by Universidad De Las Palmas De Gran Canaria, Wiley Online Library on [01/08/2025]. See the Terms and Conditions (https://onlinelibrary.wiley.com/terms-and-conditions) on Wiley Online Library for rules of use; OA articles are governed by the applicable Creative Commons License

Arístegui, J., Barton, E. D., Álvarez-Salgado, X. A., Santos, A. M. P., Figueiras, F. G., Kifani, S., et al. (2009). Sub-regional ecosystem variability in the Canary current upwelling. *Progress in Oceanography*, *83*(1–4), 33–48. https://doi.org/10.1016/J.POCEAN.2009.07.031

Bachi, G., Morelli, E., Gonnelli, M., Balestra, C., Casotti, R., Evangelista, V., et al. (2023). Fluorescent properties of marine phytoplankton exudates and lability to marine heterotrophic prokaryotes degradation. *Limnology & Oceanography*, *68*(4), 982–1000. https://doi.org/10.1002/LNO.12325

Benner, R., & Amon, R. M. W. (2015). The size-reactivity continuum of major bioelements in the ocean. *Annual Reviews*, *7*(1), 185–205. https://doi.org/10.1146/ANNUREV-MARINE-010213-135126

Bory, A. J.-M., & Newton, P. P. (2000). Transport of airborne lithogenic material Down through the water column in two contrasting regions of the eastern subtropical North Atlantic Ocean. *Global Biogeochemical Cycles*, *14*(1), 297–315. https://doi.org/10.1029/1999GB900098

Bro, R. (1997). PARAFAC. Tutorial and applications. *Chemometrics and Intelligent Laboratory Systems*, *38*(2), 149–171. https://doi.org/10.1016/S0169-7439(97)00032-4

Burgoa, N., Machín, F., Rodríguez-Santana, Á., Marrero-Diáz, Á., Álvarez-Salgado, X. A., Fernández-Castro, B., et al. (2021). Cape Verde frontal zone in summer 2017: Lateral transports of mass, dissolved oxygen and inorganic nutrients. *Ocean Science*, *17*(3), 769–788. https://doi.org/10.5194/OS-17-769-2021

Campanero, R., Burgoa, N., Fernández-Castro, B., Valiente, S., Nieto-Cid, M., Martínez-Pérez, A. M., et al. (2022). High-resolution variability of dissolved and suspended organic matter in the Cape Verde frontal zone. *Frontiers in Marine Science*, *9*, 1006432. https://doi.org/10.3389/FMARS.2022.1006432/BIBTEX

Catalá, T. S., Martínez-Pérez, A. M., Nieto-Cid, M., Álvarez, M., Otero, J., Emelianov, M., et al. (2018). Dissolved Organic Matter (DOM) in the open Mediterranean Sea. I. Basin–wide distribution and drivers of chromophoric DOM. *Progress in Oceanography*, *165*, 35–51. https://doi.org/10.1016/J.POCEAN.2018.05.002

Catalá, T. S., Reche, I., Fuentes-Lema, A., Romera-Castillo, C., Nieto-Cid, M., Ortega-Retuerta, E., et al. (2015). Turnover time of fluorescent dissolved organic matter in the dark global ocean. *Nature Communications*, *6*(1), 1–9. https://doi.org/10.1038/ncomms6986

Catalá, T. S., Reche, I., Ramón, C. L., López-Sanz, À., Álvarez, M., Calvo, E., & Álvarez-Salgado, X. A. (2016). Chromophoric signatures of microbial by-products in the dark ocean. *Geophysical Research Letters*, *43*(14), 7639–7648. https://doi.org/10.1002/2016GL069878

Cetinić, I., Perry, M. J., Briggs, N. T., Kallin, E., D'Asaro, E. A., Lee, C. M., et al. (2012). Particulate organic carbon and inherent optical properties during 2008 North Atlantic Bloom experiment. *Journal of Geophysical Research: Oceans*, *117*(C6), C06028. https://doi.org/10.1029/2011JC007771

Chen, M., Kim, J. H., Nam, S. I. L., Niessen, F., Hong, W. L., Kang, M. H., & Hur, J. (2016). Production of fluorescent dissolved organic matter in Arctic Ocean sediments. *Scientific Reports 2016*, *6*(1), 1–10. https://doi.org/10.1038/srep39213

Coble, P. G. (1996). Characterization of marine and terrestrial DOM in seawater using excitation-emission matrix spectroscopy. *Marine Chemistry*, *51*(4), 325–346. https://doi.org/10.1016/0304-4203(95)00062-3

Coble, P. G. (2007). Marine optical biogeochemistry: The chemistry of ocean color. *Chemical Reviews*, *107*(2), 402–418. https://doi.org/10.1021/cr050350+

Dahlén, J., Bertilsson, S., & Pettersson, C. (1996). Effects of UV-A irradiation on dissolved organic matter in humic surface waters. *Environment International*, *22*(5), 501–506. https://doi.org/10.1016/0160-4120(96)00038-4

Del Vecchio, R., & Blough, N. V. (2004). On the origin of the optical properties of humic substances. *Environmental Science and Technology*, *38*(14), 3885–3891. https://doi.org/10.1021/es049912h

Devresse, Q., Becker, K. W., Dilmahamod, A. F., Ortega-Retuerta, E., & Engel, A. (2023). Dissolved organic matter fluorescence as a tracer of upwelling and microbial activities in two cyclonic eddies in the Eastern tropical north Atlantic. *Journal of Geophysical Research: Oceans*, *128*(8), e2023JC019821. https://doi.org/10.1029/2023JC019821

Doval, M. D., Álvarez-Salgado, X. A., Gasol, J. M., Lorenzo, L. M., Mirón, I., Figueiras, F. G., & Pedrós-Alió, C. (2001). Dissolved and suspended organic carbon in the Atlantic sector of the Southern Ocean. Stock dynamics in upper ocean waters. *Marine Ecology Progress Series*, *223*, 27–38. https://doi.org/10.3354/MEPS223027

Engelhaupt, E., Bianchi, T. S., Wetzel, R. G., & Tarr, M. A. (2003). Photochemical transformations and bacterial utilization of high-molecular-weight dissolved organic carbon in a southern Louisiana tidal stream (Bayou Trepagnier). *Biogeochemistry*, *62*(1), 39–58. https://doi.org/10.1023/A:1021176531598

Fernández-Castro, B., Mouriño-Carballido, B., & Álvarez-Salgado, X. A. (2019). Non-redfieldian mesopelagic nutrient remineralization in the eastern North Atlantic subtropical gyre. *Progress in Oceanography*, *171*, 136–153. https://doi.org/10.1016/J.POCEAN.2018.12.001

Ferretto, N., Tedetti, M., Guigue, C., Mounier, S., Redon, R., & Goutx, M. (2014). Identification and quantification of known polycyclic aromatic hydrocarbons and pesticides in complex mixtures using fluorescence excitation–emission matrices and parallel factor analysis. *Chemosphere*, *107*, 344–353. https://doi.org/10.1016/J.CHEMOSPHERE.2013.12.087

Fichot, C. G., & Benner, R. (2012). The spectral slope coefficient of chromophoric dissolved organic matter (S275–295) as a tracer of terrigenous dissolved organic carbon in river-influenced ocean margins. *Limnology & Oceanography*, *57*(5), 1453–1466. https://doi.org/10.4319/LO.2012.57.5.1453

Fischer, G., & Karakaş, G. (2009). Sinking rates and ballast composition of particles in the Atlantic Ocean: Implications for the organic carbon fluxes to the deep ocean. *Biogeosciences*, *6*(1), 85–102. https://doi.org/10.5194/BG-6-85-2009

Fischer, G., Reuter, C., Karakas, G., Nowald, N., & Wefer, G. (2009). Offshore advection of particles within the cape blanc filament, Mauritania: Results from observational and modelling studies. *Progress in Oceanography*, *83*(1–4), 322–330. https://doi.org/10.1016/J.POCEAN.2009.07.023

Fischer, G., Romero, O., Merkel, U., Donner, B., Iversen, M., Nowald, N., et al. (2016). Deep ocean mass fluxes in the coastal upwelling off Mauritania from 1988 to 2012: Variability on seasonal to decadal timescales. *Biogeosciences*, *13*(10), 3071–3090. https://doi.org/10.5194/BG-13-3071-2016

Fischer, G., Romero, O., Toby, E., Iversen, M., Donner, B., Mollenhauer, G., et al. (2019). Changes in the dust-influenced biological carbon pump in the canary current system: Implications from a coastal and an offshore sediment trap record off cape Blanc, Mauritania. *Global Biogeochemical Cycles*, *33*(8), 1100–1128. https://doi.org/10.1029/2019GB006194

Gabric, A. J., Garcia, L., Van Camp, L., Nykjaer, L., Eifler, W., & Schrimpf, W. (1993). Offshore export of shelf production in the cape Blanc (Mauritania) giant filament as derived from coastal zone color scanner imagery. *Journal of Geophysical Research*, *98*(C3), 4697–4712. https://doi.org/10.1029/92JC01714

Gómez-Letona, M., Arístegui, J., Hernández-Hernández, N., Álvarez-Salgado, X. A., Álvarez, M., Delgadillo, E., et al. (2022). Deep ocean prokaryotes and fluorescent dissolved organic matter reflect the history of the water masses across the Atlantic Ocean. *Progress in Oceanography*, *205*, 102819. https://doi.org/10.1016/J.POCEAN.2022.102819

21699291, 2025, 7, Downloaded from https://agupubs.onlinelibrary.wiley.com/doi/10.1029/2024JC022068 by Universidad De Las Palmas De Gran Canaria, Wiley Online Library on [01/08/2025]. See the Terms and Conditions (https://onlinelibrary.wiley.com/terms-and-conditions) on Wiley Online Library for rules of use; OA articles are governed by the applicable Creative Commons License

Hansell, D. A. (2013). Recalcitrant dissolved organic carbon fractions. *Annual Review of Marine Science*, *5*(1), 421–445. https://doi.org/10.1146/annurev-marine-120710-100757

Hansen, H. P., & Koroleff, F. (1999). *Methods of seawater analysis 3rd, completely revised and extended edition* (Ed.). K. Grashoff, et al. Wiley. https://doi.org/10.1002/9783527613984

Helmke, P., Romero, O., & Fischer, G. (2005). Northwest African upwelling and its effect on offshore organic carbon export to the deep sea. *Global Biogeochemical Cycles*, *19*(4). https://doi.org/10.1029/2004GB002265

Helms, J. R., Stubbins, A., Ritchie, J. D., Minor, E. C., Kieber, D. J., & Mopper, K. (2008). Absorption spectral slopes and slope ratios as indicators of molecular weight, source, and photobleaching of chromophoric dissolved organic matter. *Limnology & Oceanography*, *53*(3), 955–969. https://doi.org/10.4319/LO.2008.53.3.0955

Holm-Hansen, O., Lorenzen, C. J., Holmes, R. W., & Strickland, J. D. H. (1965). Fluorometric determination of chlorophyll. *ICES Journal of Marine Science*, *30*(1), 3–15. https://doi.org/10.1093/ICESJMS/30.1.3

Iuculano, F., álverez-Salgado, X. A., Otero, J., Catalá, T. S., Sobrino, C., Duarte, C. M., & Agustí, S. (2019). Patterns and drivers of UV absorbing chromophoric dissolved organic matter in the euphotic layer of the open ocean. *Frontiers in Marine Science*, *6*(JUN), 449450. https://doi.org/10.3389/fmars.2019.00320

Jiao, N., Herndl, G. J., Hansell, D. A., Benner, R., Kattner, G., Wilhelm, S. W., et al. (2010). Microbial production of recalcitrant dissolved organic matter: Long-term carbon storage in the global ocean. *Nature Reviews Microbiology*, *8*(8), 593–599. https://doi.org/10.1038/nrmicro2386

Jørgensen, L., Stedmon, C. A., Kragh, T., Markager, S., Middelboe, M., & Søndergaard, M. (2011). Global trends in the fluorescence characteristics and distribution of marine dissolved organic matter. *Marine Chemistry*, *126*(1–4), 139–148. https://doi.org/10.1016/J.MARCHEM.2011.05.002

Karakaş, G., Nowald, N., Blaas, M., Marchesiello, P., Frickenhaus, S., & Schlitzer, R. (2006). High-resolution modeling of sediment erosion and particle transport across the northwest African shelf. *Journal of Geophysical Research*, *111*(C6), 6025. https://doi.org/10.1029/2005JC003296

Karstensen, J., & Tomczak, M. (1998). Age determination of mixed water masses using CFC and oxygen data. *Journal of Geophysical Research*, *103*(C9), 18599–18609. https://doi.org/10.1029/98JC00889

Kim, J., & Kim, G. (2016). Significant anaerobic production of fluorescent dissolved organic matter in the deep east sea (Sea of Japan). *Geophysical Research Letters*, *43*(14), 7609–7616. https://doi.org/10.1002/2016GL069335

Kim, J., Kim, Y., Kang, H. W., Kim, S. H., Rho, T. K., & Kang, D. J. (2020). Tracing water mass fractions in the deep Western Indian Ocean using fluorescent dissolved organic matter. *Marine Chemistry*, *218*, 103720. https://doi.org/10.1016/J.MARCHEM.2019.103720

Kothawala, D. N., Murphy, K. R., Stedmon, C. A., Weyhenmeyer, G. A., & Tranvik, L. J. (2013). Inner filter correction of dissolved organic matter fluorescence. *Limnology and Oceanography: Methods*, *11*(12), 616–630. https://doi.org/10.4319/LOM.2013.11.616

Kowalczuk, P., Tilstone, G. H., Zabłocka, M., Röttgers, R., & Thomas, R. (2013). Composition of dissolved organic matter along an Atlantic meridional transect from fluorescence spectroscopy and parallel factor analysis. *Marine Chemistry*, *157*, 170–184. https://doi.org/10.1016/J.MARCHEM.2013.10.004

Langdon, C. (2010). Determination of dissolved oxygen in seawater by Winkler titration using the amperometric technique. In E. Hood, C. Sabine, & B. Sloyan (Eds.), *The GO-SHIP repeat hydrography manual: A collection of expert reports and guidelines*. ICPO Publication Series Number 134. https://doi.org/10.25607/OBP-1350

Linke, C., Möhler, O., Veres, A., Mohácsi, Á., Bozóki, Z., Szabó, G., & Schnaiter, M. (2006). Optical properties and mineralogical composition of different Saharan mineral dust samples: A laboratory study. *Atmospheric Chemistry and Physics*, *6*(11), 3315–3323. https://doi.org/10.5194/ACP-6-3315-2006

Loginova, A. N., Dale, A. W., Le Moigne, F. A. C., Thomsen, S., Sommer, S., Clemens, D., et al. (2020). Sediment release of dissolved organic matter to the oxygen minimum zone off Peru. *Biogeosciences*, *17*(18), 4663–4679. https://doi.org/10.5194/BG-17-4663-2020

Lønborg, C., & Álvarez-Salgado, X. A. (2014). Tracing dissolved organic matter cycling in the eastern boundary of the temperate North Atlantic using absorption and fluorescence spectroscopy. *Deep Sea Research Part I: Oceanographic Research Papers*, *85*, 35–46. https://doi.org/10.1016/J.DSR.2013.11.002

Lønborg, C., Yokokawa, T., Herndl, G. J., & Antón Álvarez-Salgado, X. (2015). Production and degradation of fluorescent dissolved organic matter in surface waters of the eastern north Atlantic Ocean. *Deep Sea Research Part I: Oceanographic Research Papers*, *96*, 28–37. https://doi.org/10.1016/J.DSR.2014.11.001

Lopez, C. N., Robert, M., Galbraith, M., Bercovici, S. K., Orellana, M. V., & Hansell, D. A. (2020). High temporal variability of total organic carbon in the deep northeastern Pacific. *Frontiers in Earth Science*, *8*, 511490. https://doi.org/10.3389/FEART.2020.00080/BIBTEX

Lovecchio, E., Gruber, N., & Münnich, M. (2018). Mesoscale contribution to the long-range offshore transport of organic carbon from the canary upwelling system to the open North Atlantic. *Biogeosciences*, *15*(16), 5061–5091. https://doi.org/10.5194/BG-15-5061-2018

Martínez-Marrero, A., Rodríguez-Santana, A., Hernández-Guerra, A., Fraile-Nuez, E., López-Laatzen, F., Vélez-Belchí, P., & Parrilla, G. (2008). Distribution of water masses and diapycnal mixing in the Cape Verde frontal zone. *Geophysical Research Letters*, *35*(7). https://doi.org/10.1029/2008GL033229

Martínez-Pérez, A. M., Catalá, T. S., Nieto-Cid, M., Otero, J., Álvarez, M., Emelianov, M., et al. (2019). Dissolved Organic Matter (DOM) in the open Mediterranean Sea. II: Basin–wide distribution and drivers of fluorescent DOM. *Progress in Oceanography*, *170*, 93–106. https://doi.org/10.1016/J.POCEAN.2018.10.019

Matzenbacher, B. A., Brummer, G. J. A., Prins, M. A., & Stuut, J. B. W. (2024). High-resolution sampling in the eastern tropical North Atlantic reveals episodic Saharan dust deposition: Implications for the marine carbon sink. *Frontiers in Marine Science*, *11*, 1367786. https://doi.org/10.3389/FMARS.2024.1367786

Mbaye, M. L., Gaye, A. T., Spitzy, A., Dähnke, K., Afouda, A., & Gaye, B. (2016). Seasonal and spatial variation in suspended matter, organic carbon, nitrogen, and nutrient concentrations of the Senegal River in West Africa. *Limnologica*, *57*, 1–13. https://doi.org/10.1016/J.LIMNO.2015.12.003

McCave, I. N. (1986). Local and global aspects of the bottom nepheloid layers in the world ocean. *Netherlands Journal of Sea Research*, *20*(2–3), 167–181. https://doi.org/10.1016/0077-7579(86)90040-2

Meunier, T., Barton, E. D., Barreiro, B., & Torres, R. (2012). Upwelling filaments off cap blanc: Interaction of the NW African upwelling current and the Cape Verde frontal zone eddy field? *Journal of Geophysical Research*, *117*(C8), 8031. https://doi.org/10.1029/2012JC007905

Murphy, K. R., Butler, K. D., Spencer, R. G. M., Stedmon, C. A., Boehme, J. R., & Aiken, G. R. (2010). Measurement of dissolved organic matter fluorescence in aquatic environments: An interlaboratory comparison. *Environmental Science and Technology*, *44*(24), 9405–9412. https://doi.org/10.1021/es102362t

Murphy, K. R., Stedmon, C. A., Graeber, D., & Bro, R. (2013). Fluorescence spectroscopy and multi-way techniques. PARAFAC. *Analytical Methods*, *5*(23), 6557–6566. https://doi.org/10.1039/C3AY41160E

21699291, 2025, 7, Downloaded from https://agupubs.onlinelibrary.wiley.com/doi/10.1029/2024JC022068 by Universidad De Las Palmas De Gran Canaria, Wiley Online Library on [01/08/2025]. See the Terms and Conditions (https://onlinelibrary.wiley.com/terms-and-conditions) on Wiley Online Library for rules of use; OA articles are governed by the applicable Creative Commons License

Murphy, K. R., Stedmon, C. A., Wenig, P., & Bro, R. (2014). OpenFluor– an online spectral library of auto-fluorescence by organic compounds in the environment. *Analytical Methods*, *6*(3), 658–661. https://doi.org/10.1039/C3AY41935E

Nelson, N. B., Carlson, C. A., & Steinberg, D. K. (2004). Production of chromophoric dissolved organic matter by Sargasso Sea microbes. *Marine Chemistry*, *89*(1–4), 273–287. https://doi.org/10.1016/J.MARCHEM.2004.02.017

Nelson, N. B., Siegel, D. A., & Michaels, A. F. (1998). Seasonal dynamics of colored dissolved material in the Sargasso Sea. *Deep Sea Research Part I: Oceanographic Research Papers*, *45*(6), 931–957. https://doi.org/10.1016/S0967-0637(97)00106-4

Nieto-Cid, M., Álvarez-Salgado, X. A., & Pérez, F. F. (2006). Microbial and photochemical reactivity of fluorescent dissolved organic matter in a coastal upwelling system. *Limnology & Oceanography*, *51*(3), 1391–1400. https://doi.org/10.4319/LO.2006.51.3.1391

Ohde, T., Fiedler, B., & Körtzinger, A. (2015). Spatio-temporal distribution and transport of particulate matter in the eastern tropical north Atlantic observed by Argo floats. *Deep Sea Research Part I: Oceanographic Research Papers*, *102*, 26–42. https://doi.org/10.1016/J.DSR.2015.04.007

Pastor, M. V., Vélez-Belchí, P., & Hernández-Guerra, A. (2015). Water masses in the canary current large marine ecosystem. In L. Valdés & I. Déniz-González (Eds.), *Oceanographic and biological features in the canary current large marine ecosystem* (Vol. No 115, pp. 73–79). IOC-UNESCO. (IOC Technical Series.

Pelegrí, J. L., Marrero-Díaz, A., & Ratsimandresy, A. W. (2006). Nutrient irrigation of the north Atlantic. *Progress in Oceanography*, *70*(2–4), 366–406. https://doi.org/10.1016/J.POCEAN.2006.03.018

Pelegrí, J. L., & Peña-Izquierdo, J. (2015a). Eastern boundary currents off North-West Africa. In L. Valdés & I. Déniz-González (Eds.), *Oceanographic and biological features in the canary current large marine ecosystem (IOC technical series* (pp. 81–92). IOC-UNESCO.

Pelegrí, J. L., & Peña-Izquierdo, J. (2015b). Inorganic nutrients and dissolved oxygen in the canary current large marine ecosystem. In L. Valdés & I. Déniz-González (Eds.), *Oceanographic and biological features in the canary current large Marine ecosystem (IOC technical series* (pp. 133–142). IOC-UNESCO.

Pérez-Rodríguez, P., Pelegrí, J. L., & Marrero-Díaz, A. (2001). Dynamical characteristics of the Cape Verde frontal zone. *Scientia Marina*, *65*(S1), 241–250. https://doi.org/10.3989/SCIMAR.2001.65S1241

Romera-Castillo, C., Sarmento, H., Alvarez-Salgado, X. A. Á., Gasol, J. M., & Marrasé, C. (2011). Net production and consumption of fluorescent colored dissolved organic matter by natural bacterial assemblages growing on marine phytoplankton exudates. *Applied and Environmental Microbiology*, *77*(21), 7490–7498. https://doi.org/10.1128/AEM.00200-11

Ruiz-González, C., Mestre, M., Estrada, M., Sebastián, M., Salazar, G., Agustí, S., et al. (2020). Major imprint of surface plankton on deep ocean prokaryotic structure and activity. *Molecular Ecology*, *29*(10), 1820–1838. https://doi.org/10.1111/MEC.15454

Santana-Falcón, Y., Mason, E., & Arístegui, J. (2020). Offshore transport of organic carbon by upwelling filaments in the canary current system. *Progress in Oceanography*, *186*, 102322. https://doi.org/10.1016/J.POCEAN.2020.102322

Stedmon, C. A., & Markager, S. (2005a). Tracing the production and degradation of autochthonous fractions of dissolved organic matter by fluorescence analysis. *Limnology & Oceanography*, *50*(5), 1415–1426. https://doi.org/10.4319/LO.2005.50.5.1415

Stedmon, C. A., & Markager, S. (2005b). Resolving the variability in dissolved organic matter fluorescence in a temperate Estuary and its catchment using PARAFAC analysis. *Limnology & Oceanography*, *50*(2), 686–697. https://doi.org/10.4319/lo.2005.50.2.0686

Schlitzer, R. (2017). Ocean data view. https://odv.awi.de

Siegel, D. A., Maritorena, S., Nelson, N. B., & Behrenfeld, M. J. (2005). Independence and interdependencies among global ocean color properties: Reassessing the bio-optical assumption. *Journal of Geophysical Research*, *110*(C7), 1–14. https://doi.org/10.1029/2004JC002527

Simon, M., Grossart, H. P., Schweitzer, B., & Ploug, H. (2002). Microbial ecology of organic aggregates in aquatic ecosystems. *Aquatic Microbial Ecology*, *28*(2), 175–211. https://doi.org/10.3354/AME028175

Smith, D. C., Simon, M., Alldredge, A. L., & Azam, F. (1992). Intense hydrolytic enzyme activity on marine aggregates and implications for rapid particle dissolution. *Nature*, *359*(6391), 139–142. https://doi.org/10.1038/359139a0

Stedmon, C. A., & Bro, R. (2008). Characterizing dissolved organic matter fluorescence with parallel factor analysis: A tutorial. *Limnology and Oceanography: Methods*, *6*(11), 572–579. https://doi.org/10.4319/LOM.2008.6.572

Stedmon, C. A., Markager, S., & Bro, R. (2003). Tracing dissolved organic matter in aquatic environments using a new approach to fluorescence spectroscopy. *Marine Chemistry*, *82*(3–4), 239–254. https://doi.org/10.1016/S0304-4203(03)00072-0

Stedmon, C. A., & Nelson, N. B. (2015). The optical properties of DOM in the ocean. In D. Hansell & C. Carlson (Eds.), *Biogeochemistry of marine dissolved organic matter* (2nd ed., pp. 481–508). Academic Press. https://doi.org/10.1016/B978-0-12-405940-5.00010-8

Stedmon, C. A., & Yamashita, Y. (2024). Tracing DOM in the ocean with UV-visible spectroscopy. In D. Hansell & C. Carlson (Eds.), *Biogeochemistry of marine dissolved organic matter* (3rd ed., pp. 101–136). Elsevier. https://doi.org/10.1016/B978-0-443-13858-4.00005-8

Swan, C. M., Nelson, N. B., Siegel, D. A., & Kostadinov, T. S. (2012). The effect of surface irradiance on the absorption spectrum of chromophoric dissolved organic matter in the global ocean. *Deep Sea Research Part I: Oceanographic Research Papers*, *63*, 52–64. https://doi.org/10.1016/J.DSR.2012.01.008

Timko, S. A., Maydanov, A., Pittelli, S. L., Conte, M. H., Cooper, W. J., Koch, B. P., et al. (2015). Depth-dependent photodegradation of marine dissolved organic matter. *Frontiers in Marine Science*, *2*(SEP), 159757. https://doi.org/10.3389/FMARS.2015.00066/BIBTEX

Twardowski, M. S., & Donaghay, P. L. (2002). Photobleaching of aquatic dissolved materials: Absorption removal, spectral alteration, and their interrelationship. *Journal of Geophysical Research*, *107*(C8), 6-1. https://doi.org/10.1029/1999JC000281

UNESCO. (1985). The International System of Units (SI) in oceanography. *Technical Papers in Marine Science*, *45*, 1–124.

UNESCO. (1986). Progress on oceanographic tables and standards 1983–1986. Work and recommendations of the UNESCO/SCOR/ICES/IAPSO joint panel. *Technical Papers in Marine Science*, *50*, 1–59.

Valiente, S., Fernández-Castro, B., Campanero, R., Marrero-Díaz, A., Rodríguez-Santana, A., Gelado-Cabellero, M. D., et al. (2022). Dissolved and suspended organic matter dynamics in the Cape Verde frontal zone (NW Africa). *Progress in Oceanography*, *201*, 102727. https://doi.org/10.1016/J.POCEAN.2021.102727

van der Jagt, H., Friese, C., Stuut, J. B. W., Fischer, G., & Iversen, M. H. (2018). The ballasting effect of Saharan dust deposition on aggregate dynamics and carbon export: Aggregation, settling, and scavenging potential of marine snow. *Limnology & Oceanography*, *63*(3), 1386–1394. https://doi.org/10.1002/LNO.10779

Xiao, X., Yamashita, Y., Gonsior, M., & Jiao, N. (2023). The efficiency of the microbial carbon pump as seen from the relationship between apparent oxygen utilization and fluorescent dissolved organic matter. *Progress in Oceanography*, *210*, 102929. https://doi.org/10.1016/J.POCEAN.2022.102929

Xiao, Y. H., Sara-Aho, T., Hartikainen, H., & Vähätalo, A. V. (2013). Contribution of ferric iron to light absorption by chromophoric dissolved organic matter. *Limnology & Oceanography*, *58*(2), 653–662. https://doi.org/10.4319/LO.2013.58.2.0653

Yamashita, Y., Nosaka, Y., Suzuki, K., Ogawa, H., Takahashi, K., & Saito, H. (2013). Photobleaching as a factor controlling spectral characteristics of chromophoric dissolved organic matter in Open Ocean. *Biogeosciences*, *10*(11), 7207–7217. https://doi.org/10.5194/BG-10-7207-2013

21699291, 2025, 7, Downloaded from https://agupubs.onlinelibrary.wiley.com/doi/10.1029/2024JC022068 by Universidad De Las Palmas De Gran Canaria, Wiley Online Library on [01/08/2025]. See the Terms and Conditions (https://onlinelibrary.wiley.com/terms-and-conditions) on Wiley Online Library for rules of use; OA articles are governed by the applicable Creative Commons License

Yamashita, Y., Boyer, J. N., & Jaffé, R. (2013). Evaluating the distribution of terrestrial dissolved organic matter in a complex coastal ecosystem using fluorescence spectroscopy. *Continental Shelf Research*, *66*, 136–144. https://doi.org/10.1016/j.csr.2013.06.010

Yamashita, Y., & Tanoue, E. (2008). Production of bio-refractory fluorescent dissolved organic matter in the ocean interior. *Nature Geoscience*, *1*(9), 579–582. https://doi.org/10.1038/ngeo279

Zenk, W., Klein, B., & Schroder, M. (1991). Cape Verde frontal zone. *Deep-Sea Research, Part A: Oceanographic Research Papers*, *38*, S505–S530. https://doi.org/10.1016/S0198-0149(12)80022-7

References From the Supporting Information

Andersson, M. G. I., Catalán, N., Rahman, Z., Tranvik, L. J., & Lindström, E. S. (2018). Effects of sterilization on Dissolved Organic Carbon (DOC) composition and bacterial utilization of DOC from Lakes. *Aquatic Microbial Ecology*, *82*(2), 199–208. https://doi.org/10.3354/ame01890

Angelotti de Ponte Rodrigues, N., Carmigniani, R., Guillot-Le Goff, A., Lucas, F. S., Therial, C., Naloufi, M., et al. (2024). Fluorescence spectroscopy for tracking microbiological contamination in urban waterbodies. *Frontiers in Water*, *6*. https://doi.org/10.3389/frwa.2024.1358483

Borisover, M., Laor, Y., Parparov, A., Bukhanovsky, N., & Lado, M. (2009). Spatial and seasonal patterns of fluorescent organic matter in Lake Kinneret (sea of Galilee) and its catchment basin. *Water Research*, *43*(12), 3104–3116. https://doi.org/10.1016/j.watres.2009.04.039

Hambly, A. C., Arvin, E., Pedersen, L.-F., Pedersen, P. B., Seredyńska-Sobecka, B., & Stedmon, C. A. (2015). Characterising organic matter in recirculating aquaculture systems with fluorescence EEM spectroscopy. *Water Research*, *83*, 112–120. https://doi.org/10.1016/j.watres.2015.06.037

Kothawala, D. N., Stedmon, C. A., Müller, R. A., Weyhenmeyer, G. A., Köhler, S. J., & Tranvik, L. J. (2014). Controls of dissolved organic matter quality: Evidence from a large-scale boreal Lake survey. *Global Change Biology*, *20*(4), 1101–1114. https://doi.org/10.1111/gcb.12488

Kowalczuk, P., Durako, M. J., Young, H., Kahn, A. E., Cooper, W. J., & Gonsior, M. (2009). Characterization of dissolved organic matter fluorescence in the South Atlantic bight with use of PARAFAC model: Interannual variability. *Marine Chemistry*, *113*(3–4), 182–196. https://doi.org/10.1016/j.marchem.2009.01.015

Krylov, I. N., Drozdova, A. N., & Labutin, T. A. (2020). Albatross R package to study PARAFAC components of DOM fluorescence from mixing zones of arctic shelf seas. *Chemometrics and Intelligent Laboratory Systems*, *207*, 104176. https://doi.org/10.1016/j.chemolab.2020.104176

Lambert, T., Bouillon, S., Darchambeau, F., Massicotte, P., & Borges, A. V. (2016). Shift in the chemical composition of dissolved organic matter in the Congo River network. *Biogeosciences*, *13*(18), 5405–5420. https://doi.org/10.5194/bg-13-5405-2016

Logozzo, L. A., Hosen, J. D., McArthur, J., & Raymond, P. A. (2023). Distinct drivers of two size fractions of operationally dissolved iron in a temperate river. *Limnology & Oceanography*, *68*(6), 1185–1200. https://doi.org/10.1002/lno.12338

Maurischat, P., Lehnert, L., Zerres, V. H. D., Tran, T. V., Kalbitz, K., Rinnan, Å., et al. (2022). The glacial–terrestrial–fluvial pathway: A multiparametrical analysis of spatiotemporal dissolved organic matter variation in three catchments of Lake Nam Co, Tibetan Plateau. *Science of The Total Environment*, *838*, 156542. https://doi.org/10.1016/j.scitotenv.2022.156542

Murphy, K. R., Bro, R., & Stedmon, C. A. (2014). Chemometric analysis of organic matter fluorescence. In P. Coble, A. Baker, J. Lead, D. Reynolds, & R. Spencer (Eds.), *Aquatic organic matter fluorescence*. Cambridge University Press.

Murphy, K. R., Timko, S. A., Gonsior, M., Powers, L. C., Wünsch, U. J., & Stedmon, C. A. (2018). Photochemistry illuminates ubiquitous organic matter fluorescence spectra. *Environmental Science and Technology*, *52*(19), 11243–11250. https://doi.org/10.1021/acs.est.8b02648

Osburn, C. L., Boyd, T. J., Montgomery, M. T., Bianchi, T. S., Coffin, R. B., & Paerl, H. W. (2016). Optical proxies for terrestrial dissolved organic matter in estuaries and coastal waters. *Frontiers in Marine Science*, *127*. https://doi.org/10.3389/fmars.2015.00127

Osburn, C. L., Mikan, M. P., Etheridge, J. R., Burchell, M. R., & Birgand, F. (2015). Seasonal variation in the quality of dissolved and particulate organic matter exchanged between a salt marsh and its adjacent Estuary. *Journal of Geophysical Research: Biogeosciences*, *120*(7), 1430–1449. https://doi.org/10.1002/2014JG002897

Osburn, C. L., Oviedo-Vargas, D., Barnett, E., Dierick, D., Oberbauer, S. F., & Genereux, D. P. (2018). Regional groundwater and storms are hydrologic controls on the quality and export of dissolved organic matter in two tropical rainforest streams, Costa Rica. *Journal of Geophysical Research: Biogeosciences*, *123*(3), 850–866. https://doi.org/10.1002/2017JG003960

Podgorski, D. C., Walley, J., Shields, M. P., Hebert, D., Harsha, M. L., Spencer, R. G. M., et al. (2024). Dispersant-enhanced photodissolution of macondo crude oil: A molecular perspective. *Journal of Hazardous Materials*, *461*, 132558. https://doi.org/10.1016/j.jhazmat.2023.132558

Retelletti Brogi, S., Balestra, C., Casotti, R., Cossarini, G., Galletti, Y., Gonnelli, M., et al. (2020). Time resolved data unveils the complex DOM dynamics in a Mediterranean river. *Science of The Total Environment*, *733*, 139212. https://doi.org/10.1016/j.scitotenv.2020.139212

Retelletti Brogi, S., Cossarini, G., Bachi, G., Balestra, C., Camatti, E., Casotti, R., et al. (2022). Evidence of Covid-19 lockdown effects on riverine dissolved organic matter dynamics provides a proof-of-concept for needed regulations of anthropogenic emissions. *Science of The Total Environment*, *812*, 152412. https://doi.org/10.1016/j.scitotenv.2021.152412

Schittich, A.-R., Wünsch, U. J., Kulkarni, H. V., Battistel, M., Bregnhøj, H., Stedmon, C. A., & McKnight, U. S. (2018). Investigating fluorescent organic-matter composition as a key predictor for arsenic mobility in groundwater aquifers. *Environmental Science and Technology*, *52*(22), 13027–13036. https://doi.org/10.1021/acs.est.8b04070

Shutova, Y., Baker, A., Bridgeman, J., & Henderson, R. K. (2014). Spectroscopic characterisation of dissolved organic matter changes in drinking water treatment: From PARAFAC analysis to online monitoring wavelengths. *Water Research*, *54*, 159–169. https://doi.org/10.1016/j.watres.2014.01.053

Smith, M. A., Kominoski, J. S., Gaiser, E. E., Price, R. M., & Troxler, T. G. (2021). Stormwater runoff and tidal flooding transform dissolved organic matter composition and increase bioavailability in urban coastal ecosystems. *Journal of Geophysical Research: Biogeosciences*, *126*(7), e2020JG006146. https://doi.org/10.1029/2020JG006146

Wang, H., Li, Z., Zhuang, W.-E., Hur, J., Yang, L., & Wang, Y. (2020). Spectral and isotopic characteristics of particulate organic matter in a subtropical Estuary under the influences of human disturbance. *Journal of Marine Systems*, *203*, 103264. https://doi.org/10.1016/j.jmarsys.2019.103264

Wang, S., Perkins, M., Matthews, D. A., & Zeng, T. (2021). Coupling suspect and nontarget screening with mass balance modeling to characterize organic micropollutants in the Onondaga lake–three Rivers system. *Environmental Science and Technology*, *55*(22), 15215–15226. https://doi.org/10.1021/acs.est.1c04699

Wang, S., Wasswa, J., Feldman, A. C., Kabenge, I., Kiggundu, N., & Zeng, T. (2022). Suspect screening to support source identification and risk assessment of organic micropollutants in the aquatic environment of a Sub-Saharan African urban center. *Water Research*, *220*, 118706. https://doi.org/10.1016/j.watres.2022.118706

21699291, 2025, 7, Downloaded from https://agupubs.onlinelibrary.wiley.com/doi/10.1029/2024JC022068 by Universidad De Las Palmas De Gran Canaria, Wiley Online Library on [01/08/2025]. See the Terms and Conditions (https://onlinelibrary.wiley.com/terms-and-conditions) on Wiley Online Library for rules of use; OA articles are governed by the applicable Creative Commons License

Wheeler, K. I., Levia, D. F., & Hudson, J. E. (2017). Tracking senescence-induced patterns in leaf litter leachate using parallel factor analysis (PARAFAC) modeling and self-organizing maps. *Journal of Geophysical Research: Biogeosciences*, *122*(9), 2233–2250. https://doi.org/10.1002/2016JG003677

Williams, C. J., Frost, P. C., & Xenopoulos, M. A. (2013). Beyond best management practices: Pelagic biogeochemical dynamics in urban stormwater ponds. *Ecological Applications*, *23*(6), 1384–1395. https://doi.org/10.1890/12-0825.1

Wünsch, U. J., Geuer, J. K., Lechtenfeld, O. J., Koch, B. P., Murphy, K. R., & Stedmon, C. A. (2018). Quantifying the impact of solid-phase extraction on chromophoric dissolved organic matter composition. *Marine Chemistry*, *207*, 33–41. https://doi.org/10.1016/j.marchem.2018.08.010

Wünsch, U. J., Murphy, K. R., & Stedmon, C. A. (2017). The one-sample PARAFAC approach reveals molecular size distributions of fluorescent components in dissolved organic matter. *Environmental Science and Technology*, *51*(20), 11900–11908. https://doi.org/10.1021/acs.est.7b03260

Zabłocka, M., Kowalczuk, P., Meler, J., Peeken, I., Dragańska-Deja, K., & Winogradow, A. (2020). Compositional differences of fluorescent dissolved organic matter in Arctic Ocean spring sea ice and surface waters north of Svalbard. *Marine Chemistry*, *227*, 103893. https://doi.org/10.1016/j.marchem.2020.103893

21699291, 2025, 7, Downloaded from https://agupubs.onlinelibrary.wiley.com/doi/10.1029/2024JC022068 by Universidad De Las Palmas De Gran Canaria, Wiley Online Library on [01/08/2025]. See the Terms and Conditions (https://onlinelibrary.wiley.com/terms-and-conditions) on Wiley Online Library for rules of use; OA articles are governed by the applicable Creative Commons License